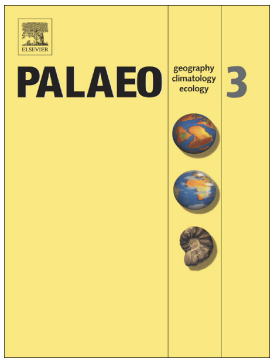

Lacustrine stromatolites as multi-scale recorders of climate change: Insights from the Miocene Ebro Basin

Leticia Martin-Bello, Concha Arenas, Julian E. Andrews, Ana M. Alonso-Zarza, Alina Marca

PII: S0031-0182(18)30770-3
DOI: https://doi.org/10.1016/j.palaeo.2019.05.001
Reference: PALAEO 9179

To appear in: *Palaeogeography, Palaeoclimatology, Palaeoecology*

Received date: 13 September 2018
Revised date: 30 April 2019
Accepted date: 1 May 2019

Please cite this article as: L. Martin-Bello, C. Arenas, J.E. Andrews, et al., Lacustrine stromatolites as multi-scale recorders of climate change: Insights from the Miocene Ebro Basin, Palaeogeography, Palaeoclimatology, Palaeoecology, https://doi.org/10.1016/j.palaeo.2019.05.001

Lacustrine stromatolites as multi-scale recorders of climate change: insights from the Miocene Ebro Basin

Leticia Martin-Bello[1*], Concha Arenas[1], Julian E. Andrews[2], Ana M. Alonso-Zarza[3], Alina Marca[2]

[1] *Department of Earth Sciences, Institute for Research on Environmental Sciences of Aragón (IUCA) and Geotransfer group, University of Zaragoza. 50009 Zaragoza, Spain*

[2] *School of Environmental Sciences, University of East Anglia, Norwich, NR4 7TJ, UK*

[3] *Department of Petrology and Geochemistry, Faculty of Geology, Complutense University of Madrid, 28040 Madrid, Spain*

*Corresponding author. E-mail address: leticia.martin.bello@gmail.com

Abstract

Sedimentological, $\delta^{13}C$ and $\delta^{18}O$ data from stromatolites in a lower and middle Miocene sequence from the Ebro Basin (N Spain) are used to assess the potential of ancient lacustrine stromatolite lamination as an archive of palaeoenvironmental and palaeoclimatic change. The isotopic evolution through the studied sequence supports a general trend toward less saline conditions with time. Stromatolites and muddy-grainy laminated limestones developed in lake water that underwent little renewal, compared with other carbonate facies. The palaeoclimatic value of the stable-isotope changes and concurrent textural variations in calcite stromatolite lamination is studied at different orders of cyclicity. Stromatolite lamination consists of simple laminae (dark dense, light dense and light porous) grouped into alternating composite light and dark laminae. $\delta^{13}C$ and $\delta^{18}O$ analyses in consecutive composite laminae (bulk sampling) yielded a cyclic pattern that mimics textural variations. Light laminae, with lower $\delta^{13}C$ and $\delta^{18}O$ values, reflect higher precipitation/evaporation ratio (P/E) and more influence of biogenic ^{12}C. Dark laminae, with higher $\delta^{13}C$ and $\delta^{18}O$ values, reflect drier conditions, more complete atmospheric CO_2 exchange with water and photosynthetic $^{12}CO_2$ uptake. Textural features of laminae support these results: the dark laminae are related to higher calcite saturation in lake water during drier periods. Isotopic values from high-resolution sampling through a 2.1-cm thick stromatolite reveal palaeoclimate variations at different temporal scales. Isotopic variation in 3rd order cyclicity of alternating light/dark simple laminae is recording seasonal P/E variations. Light and dark composite laminae (2nd order cyclicity) correspond to pluriannual dominantly-humid or -dry conditions, respectively. A gradual succession from light to dark composite laminae forms the 1st order cycles driven by decreasing P/E through longer pluriannual periods, resulting in lake level lowering. The stromatolites are thus recording lake level changes of centennial to millennial scale.

Key words: stromatolites; stable isotopes; high resolution sampling; lake level changes; cyclicity; climate changes.

1. Introduction

The stable isotopic composition of microbial carbonates is potentially a powerful record of palaeoclimatic and paleoenvironmental conditions (Casanova and Hillaire-Marcel, 1992; Andrews et al., 1993; Vasconcelos et al., 2005; Petryshyn et al., 2012). However, most studies on marine (Park, 1976; Riding, 2000; Reid et al., 2003) or continental stromatolites (Sanz-Montero et al., 2008; Oliveri et al., 2010; Frantz et al., 2014; Lettéron et al., 2018) typically focus on their diverse macro-sedimentological character rather than on finer-scale attributes

such as microbial lamination style and cyclicity. Moreover, detailed study of microbial lamination, when attempted, is commonly approached from a simple textural perspective (Adachi et al., 2017).

In this contribution we explore coupled textural and geochemical variation in microbial laminae, an approach that has so far mainly been attempted on recent or sub-recent fluvial tufa stromatolites examples (Chafetz et al., 1991; Arp et al, 2010; Brasier et al., 2010; Dabkowski et al., 2015; Osácar et al., 2017; Rodríguez-Berriguete et al., 2018), with just a few studies of Phanerozoic stromatolites (Abell et al., 1982; Nehza et al., 2009; Arenas et al., 2015) or older stromatolite examples (Beukes et al., 1989; Frank et al., 1997; Grotzinger and Knoll, 1999). Regardless of the age, the results of these studies are often not wholly satisfactory, particularly in the ancient record where there is not always consensus about the significance of the isotopic variations with time or even the environmental drivers (Kano et al., 2007; Osácar et al., 2013; López-Blanco et al., 2016).

This paper documents the concurrent textural and stable isotope changes that occur in Miocene lacustrine stromatolites of the Ebro Basin. These deposits formed in a closed lake system (Arenas and Pardo, 1999). The correlative changes are observed in laminated microfacies at three different scales of cyclicity. In this palaeolake system, stromatolites are associated with muddy-grainy laminated limestones that developed at intermediate settings between high lake level (with freshwater carbonate deposition), and low lake level (with sulphate deposition) (Arenas and Pardo, 1999). Water level in closed lakes is controlled by the balance between inputs (mostly via precipitation and ground water) and outputs (mostly through evaporation), broadly the precipitation versus evaporation ratio (P/E) (Talbot, 1990; Arp et al., 2005; Nehza et al., 2009; López-Blanco et al., 2016). P/E oscillations may in turn be recorded by changes in facies types, thickness, texture, and stable isotope composition of the lacustrine deposits on different time scales, from long-term (e.g., facies associations, macrosequences or even genetic stratigraphic units) to short-term (e.g., at the lamination scale).

The aim of this work is to decipher the depositional, hydrological and climatic conditions recorded by stromatolites, from the scale of broad (metric) facies successions through to lamination at a millimetric scale. The study uses high-resolution carbon and oxygen stable isotope ($\delta^{13}C$ and $\delta^{18}O$) data as a basis to detect the lamina arrangement orders and to elucidate the parameters controlling isotopic and textural variations of different frequency cycles.

2. Stratigraphic, sedimentological and geological setting

The Ebro Basin, in the northeastern sector of the Iberian Peninsula (Fig. 1A), represents the youngest southern foreland basin of the Pyrenean Range (Riba et al., 1983). The basin fill comprises Palaeocene to Miocene marine and continental deposits. Oligocene to Miocene deposition was endorheic with alluvial, fluvial and lacustrine sedimentation derived from the Pyrenean, Iberian and Catalan Coastal Ranges; from the middle-late Miocene the basin progressively opened to the Mediterranean Sea. One of the central uplands in the basin is the Sierra de Alcubierre, the study area for this work. The Miocene sequence of this Sierra is formed of approximately 600-m thick distal fluvial and closed lake lacustrine deposits with abundant stromatolites (Arenas et al., 1997).

The Palaeocene to Miocene succession in the Ebro Basin comprises eight tectosedimentary units (T1-T8; Muñoz et al., 2002; Pardo et al., 2004) of which units T5–T7 are present in the Sierra de Alcubierre (Fig. 1). These units comprise the Agenian to the Aragonian (equivalent to Aquitanian and Serravalian, respectively) (Muñoz et al., 2002; Pérez Rivarés, 2016). Unit T5 comprises 350 m of gypsum, marls, limestones and dolostones passing laterally into limestones and marls to the east and north and into fluvial mudstones and sandstones further north. Unit T6 comprises 135 m of limestones and marls that include gypsum beds in the southwestern part of the Sierra. Unit T7 is 110 m thick, formed of mudstone, sandstone, limestone, and marlstone. Representative stratigraphic sections are shown in Figure 2.

The sedimentary facies of the Miocene lacustrine, palustrine, and fluvial successions in the central part of the Ebro Basin, were established by Arenas (1993) and Arenas and Pardo (1999). These facies (Fig. 3; Table 1) include: massive bioclastic limestones (Lm); bioturbated limestones (Lb); laminated limestones (Ll), with lenticular or wavy stratification (Ll.1), hummocky cross-stratification (Ll.2), and parallel lamination (Ll.3); marls (M); stromatolites (Ls); massive, rippled, and cross-stratified sandstones (Sm, Sr, St); nodular gypsum (Gn); and lenticular, rippled, and laminated gypsum (Glen, Gr, Gl). Oncolites (Lo) are also found in a few sites.

One main lacustrine carbonate facies association was recognized (Arenas and Pardo, 1999): Ls-> Ll-> M (Sm)->Ll (Ls)-> Lm-> Lb, which represent deepening up to the marls, and then shallowing (Fig. 4). Bioclastic lime muds formed in freshwater and produced massive limestones (Lm). The palustrine context and pedogenesis (bioturbated limestones, Lb) are associated with shallowing from Lm settings. In contrast, more saline conditions are associated with stromatolites and laminated limestones. The facies associations (Fig. 4) thus record variations in salinity, which, in turn, are related to water level variations. These earlier interpretations were supported by facies-based bulk sample stable isotope compositions which yielded lower $\delta^{13}C$ and $\delta^{18}O$ values for facies Lm and Lb and higher values for facies Ll

and Ls (Arenas et al., 1997). Fair-weather versus storm-generated hydrodynamic conditions are also recorded by the three subfacies that compose the laminated limestones (Ll) (Arenas and Pardo, 1999). Laminated limestones with parallel lamination (Ll.3) and with lenticular or wavy stratification (Ll.1) formed in shallow lake areas during fair weather conditions. Laminated limestones with hummocky cross-stratification (Ll.2) formed under the influence of storm activity. Hydrodynamics may also influence distinct stromatolite morphologies: 1) microbial colonization after subaerial exposure and/or erosion in very shallow to subaerial conditions, giving rise to thin planar stromatolites; 2) microbial growth during fair-weather periods within general storm-dominated conditions, causing the formation of thin planar stromatolites (Ls.1), stratiform stromatolites (Ls.2) or domed stromatolites (Ls.3) (Martin-Bello et al., 2019).

3. Lamina terminology

In this paper a simple lamina is considered "the smallest unit of layering", up to 1 cm thick, with uniform texture, following Walter (1972) and Arenas and Jones (2017). In the study area, simple laminae, 0.04 to 2 mm thick, are separated from underlying and overlying laminae by boundaries that exhibit sharp and gradational changes in color and/or texture (Martin-Bello, et al., 2019). Two or more simple laminae can be grouped into a composite lamina (Fig. 5), in which one lamina type is dominant (Arenas et al., 2015; Arenas and Jones, 2017). Each composite lamina is distinguished by variations in texture and color from the overlying and underlying laminae.

4. Methods and materials

Thirty four stratigraphic sections (each ~1 m thick) containing stromatolites were measured in detail and sampled; 120 hand specimens were used to prepare thin sections that were used for textural characterization by petrographic microscope.

The mineralogy of the carbonate samples was determined by X-ray diffraction (XRD) using a D-Max Rigaku diffractometer equipped with a graphite monochromator and CuKa radiation (software JADE 7.5 Materials Data) at the *Servicio de Apoyo a la Investigación (SAI)* of the University of Zaragoza. All the samples presented in this study are calcitic with ~1 % siliciclastic sediment (mostly quartz).

Samples to investigate evolution in $\delta^{13}C$ and $\delta^{18}O$ were taken through successive beds from units T5 (succession containing VS-22) and T6 (succession containing SC-141). In addition, four stromatolite specimens from units T5 (PL-22't and VS-22), T6 (AC-9 and SC-141t), and T7 (SC-197b) were taken for isotopic analyses in consecutive laminae. A total of 82 sub-samples

were taken in the four stromatolites, with one sample taken per two or more simple laminae in the composite laminae (hereafter "bulk" samples). Around 100 μg of powdered sample was retrieved from each lamina, drilled from polished slabs using a 0.4 mm diameter micro-drill (Navfram model N120 Micromotor 25.000 rpm with electronic speed regulator). The samples were analysed on a Thermo Finnigan MAT-252 mass spectrometer at the *Serveis científico-tècnics* of the University of Barcelona (Spain). $\delta^{13}C$ and $\delta^{18}O$ were calibrated to the international reference scale Vienna Pee-Dee Belemnite (VPDB) using IAEA Certified Reference Material NBS-18 ($\delta^{13}C$ VPDB = —5.10 ‰ and $\delta^{18}O$ VPDB = —23.20 ‰) and internal laboratory standard RC-1 ($\delta^{13}C$ VPDB = +2.83 ‰ and $\delta^{18}O$ VPDB = —2.08 ‰) and CECC ($\delta^{13}C$ VPDB = —20.77 ‰ and $\delta^{18}O$ VPDB = —17.56 ‰). Results are expressed as ‰ in δ notation relative to (VPDB), with a 1σ precision of ±0.04, ±0.02, and ±0.03 ‰ for the $\delta^{13}C$, and ±0.06, ±0.09, and ±0.05 ‰ for the $\delta^{18}O$, based on 8 to 9 repeated analyses of NBS-18, RC-1 and CECC, respectively, interspersed with the unknown samples. Results are shown in supplementary Table 1.

High-resolution sampling (HRS) of specimen PL-22't was done by serial milling using a hand-held microfile. Two hundred successive samples were taken through 21.4 mm of the upper part of the specimen and were directly comparable with 6 bulk samples through the same section. The thickness of the milled samples was ~137 μm. During HRS sampling, care was taken to mill individual laminae. In most cases this was successful although where the laminae were curved, minor cross contamination at lamina boundaries was possible.

HRS and the corresponding isotopic analyses were made at the University of East Anglia Stable Isotope Laboratory, UK. The samples were reacted with 103% phosphoric acid (H_3PO_4) at 90°C in an automated common acid bath. The evolved CO_2 was purified and analysed for $\delta^{13}C$ and $\delta^{18}O$ using a Europa SIRA II dual inlet isotope ratio mass spectrometer. The data are reported on the VPDB scale using IAEA Certified Reference Material NBS-19 ($\delta^{13}C$ VPDB = +1.95 ‰ and $\delta^{18}O$ VPDB = —2.20 ‰), and internal laboratory standard UEACMST ($\delta^{13}C$ VPDB = +1.99 ‰ and $\delta^{18}O$ VPDB = —2.05 ‰). Results are expressed in δ ‰ VPDB), with a 1σ precision of ±0.05 ‰ for the $\delta^{13}C$ and the $\delta^{18}O$ based on standard replicates (8 repeated analyses within each set of samples), and are shown in supplementary Table 2.

5. Textural characteristics and lamina arrangement

The stromatolites contain mostly micritic and microsparite laminae with some minor fibrous calcite (Fig. 5; Martin-Bello et al., 2019). Four simple lamina types are present:

- Dark dense micrite laminae (0.04–0.53 mm thick): dark grey micrite with little lateral lamina thickness variation; sharp upper lamina boundaries and more

gradational lower boundaries (Fig. 5). Micrite consists of densely packed, mainly subhedral 2 μm calcite crystals and 0.3 μm anhedral rounded crystals. Small pores (up to ~50 μm long) may be elongated parallel and perpendicular to the lamination.

- Light porous/clotted micrite to microsparite laminae (0.08–1.32 mm thick): composed of micrite and microsparite forming clots or peloids (Fig. 5B); lateral lamina thickness variation most marked at dome apices. Peloids are 10–20 μm diameter, composed of rhombohedral crystals with a pseudo-radial disposition, of variable sizes and shapes, ~ 1 μm in the center and 3–5 μm near edges. Pores between peloids are 5 to 10 μm across with porosity usually increasing upward.
- Light dense micrite laminae (0.11–1.89 mm thick): light grey or brown micrite, with irregular lateral lamina thickness variation. Quartz grains and clay minerals are present along with intraclasts, bioclasts and ooids.
- Fibrous laminae (0.01–0.34 mm thick): elongate crystals with long axes perpendicular to lamination, forming a fibrous microfabric. This type of laminae occurs only alternating with dark dense micrite laminae, and grading laterally into some dome/column apices.

The principal lamina types discussed here—micrite and microsparite laminae— typically occur as alternating light and dark laminae couplets, the colour variation mainly reflecting opacity caused by differing crystal sizes and porosity (Fig. 5E, F). Pores typically remain empty, except from a 10 μm thick subhedral microsparite rim. The exception is in the San Caprasio, Barranco de la Loba, Puig Ladrón and Lasfachastis samples where gypsum crystals (poikilotopic or microcrystalline) plug porosity.

The simple micrite and microsparite laminae can combine to form two types of composite laminae:

- Dark composite laminae (DCL) (0.3–2.8 mm thick) formed of: (1) dark dense micrite laminae with intercalated thinner light porous/clotted micrite to microsparite laminae (Fig. 5A), or (2) successive dark dense micrite laminae (Fig. 5B).
- Light composite laminae (LCL) (0.6–6.4 mm thick) formed of: (1) a thick light porous lamina with thin dense dark simple lamina intercalations (Fig. 5B), or (2) an alternation of porous and light dense laminae (Fig. 5A).

Boundaries between simple laminae (including those in composite laminae) are gradational between the light dense and light porous lamina, and from light (either type) to dark laminae. Boundaries from dark to the light laminae are sharp. Lamination patterns in the stromatolites are as follows (Martin-Bello et al., 2019, based on Monty, 1967):

- Simple alternating lamination. Alternating dark dense and light porous simple laminae (Fig. 5D).
- Cyclothemic lamination. Succession of cycles, each consisting of a light dense lamina at the base, followed by a light porous simple lamina and a dark dense simple lamina at the top.
- Composite alternating lamination. Alternating dark composite laminae and light, either simple or composite, laminae (Fig. 5A, B and C). The dark and light composite laminae can be of either type (see above).

6. Results

6.1. Isotopic analyses

Facies-scale carbonate isotopic compositions have broad ranges of $\delta^{13}C$ (—6.4 ‰ < $\delta^{13}C$ VPDB < +0.4 ‰) and $\delta^{18}O$ (—9.0 ‰ < $\delta^{18}O$ VPDB < +3.9 ‰); n = 189. The lower values are those of massive and bioturbated bioclastic facies (mean —3 ‰ $\delta^{13}C$ and —6 ‰ $\delta^{18}O$; n = 32). The higher values are those of stromatolites and laminated limestones (mean —1.7 ‰ $\delta^{13}C$ and —3.2 ‰ $\delta^{18}O$; n = 145). Marls have intermediate values (mean —1.9‰ $\delta^{13}C$ and —2.5 ‰ $\delta^{18}O$; n = 12). These means (Table 2) include both the new Sierra de Alcubierre data and those of Arenas et al. (1997).

6.1.1. Stable isotopic composition of facies successions

To understand the broad environmental conditions of stromatolite growth, isotopic variation was studied in a shallowing cycle VS-21 to 24 (hereafter succession VS; Fig. 6) and a deepening cycle SC-141 to 143 (hereafter succession SC; Fig. 7). Both cycles include different facies (Lb, Lm, Ll, M, and Ls; Table 1) and are directly comparable to the facies associations of Arenas et al. (1997; Fig. 4).

In succession VS, from unit T5 (Fig. 6), $\delta^{13}C$ and $\delta^{18}O$ are broadly covariant (r = 0.8, n = 8, p = 0.01), with temporal evolution toward lower values. $\delta^{13}C$ and $\delta^{18}O$ in succession SC (unit T6, Fig. 7) are also covariant (r = 0.8, N = 9, p = 0.01) in all, but the 2 basal samples. $\delta^{18}O$ and $\delta^{13}C$ values are higher in marls and then a decrease upward to the laminated limestones and stromatolites, followed by a gradual temporal evolution toward lower values in the younger marls.

6.1.2. Bulk-sampling $\delta^{13}C$ and $\delta^{18}O$ analyses in stromatolites

Stromatolite samples included stratiform (Ls.2) types in unit T5 (Puig Ladrón and Valle de Soler sections; Fig. 8), a domed stromatolite (Ls.3, specimen AC-9, Aldea del Correo section) and a thin planar stromatolite (Ls.1, specimen SC-141t, San Caprasio section) both from unit T6 (Fig. 9), and a thin planar stromatolite (Ls.1, specimen SC-197b, San Caprasio section) from unit T7 (Fig. 10).

$\delta^{13}C$ and $\delta^{18}O$ values for successive composite light and dark stromatolite laminae in units T5 and T6 have similar ranges (Table 2) with $\delta^{13}C$ between —2 and —0.5 ‰ and $\delta^{18}O$ between —5.4 and —3 ‰. In unit T7 $\delta^{13}C$ is between —4.7 to —3.9 ‰ and $\delta^{18}O$ between —7.1 to —4.9 ‰ (Figs. 8, 9 and 10).

The $\delta^{13}C$ and $\delta^{18}O$ values of successive composite light and dark laminae in units T5 and T6 specimens (Figs. 8 and 9) are positively correlated (Table 2). They show a cyclic pattern with light composite laminae having lower values than dark composite laminae (Table 2). The $\delta^{13}C$ and $\delta^{18}O$ data from T7 are negatively correlated, with light composite laminae having higher $\delta^{13}C$ values than dark composite laminae (Table 2).

6.1.3. $\delta^{13}C$ and $\delta^{18}O$ from high-resolution sampling (HRS)

$\delta^{18}O$ and $\delta^{13}C$ values from HRS correspond to the upper part of specimen PL-22't (Fig. 8A). HRS $\delta^{18}O$ and $\delta^{13}C$ values are consistent with bulk isotopic analyses of the same specimen (Fig. 11). Individual HRS values range from —3.5 to —5.5 ‰ for $\delta^{18}O$, and from —0.3 to —1.2 ‰ for $\delta^{13}C$ (Table 2 suppl.). The $\delta^{18}O$ of light laminae are close to —5 ‰ with a minimum of —5.3 ‰, while dark laminae have higher values, close to —4 ‰, with a maximum of —3.5 ‰ (Fig. 10).

The difference between the mean HRS values of the dark and light laminae is 0.4 ‰ for $\delta^{18}O$ and 0.2 ‰ for $\delta^{13}C$. Correlation between $\delta^{18}O$ and $\delta^{13}C$ is highly significant, with $r = 0.8$ ($n = 202$, $p = 0.0005$). The trend of the HRS $\delta^{18}O$ and $\delta^{13}C$ values from base to top is toward higher values, with a net change of ~0.9 ‰ (Fig. 11B) consistent with that of the bulk samples (Fig. 11C).

7. Cyclicity of HRS isotopic values

Three scales of cyclic variation are evident from the HRS data. At higher frequency (3rd order), there are groups of consecutive lower isotopic values that correspond to light, either porous or dense, simple laminae. They alternate with groups of consecutive higher isotopic values that correspond to dark dense simple laminae (e.g. samples 66-74, 75-80 and 92-94, Fig. 11). This cyclicity is also detected at lower frequency (2nd order), at the scale of composite

laminae (LCL and DCL in Fig. 11). Groups of alternating light and dark simple laminae with higher values ($\delta^{18}O$ —5.1 to —3.5 ‰ and $\delta^{13}C$ —1.1 to —0.3 ‰), correspond to dark composite laminae (samples 11-17, 66-106 and 133-156 in Fig. 11B), while groups of alternating light and dark simple laminae with lower values ($\delta^{18}O$ —5.3 to —4.2 ‰ and $\delta^{13}C$ —1.2 to —0.4 ‰), correspond to light composite laminae (samples 1-10, 18-65, 107-132 and 157-202 in Fig. 11B). In general, the passage from dark to light composite laminae correspond to sharper isotopic changes than the more gradual isotopic changes in the passage from light to dark laminae (Fig. 11). The lowest frequency (1st order) cyclicity results from the succession of light and dark composite laminae, with increasing-upward isotopic values (Fig. 11B).

8. Overview of drivers for isotopic variability in closed lakes

The carbon and oxygen isotope compositions of carbonate sediments in lakes are controlled by a number of source and process effects.

The $\delta^{18}O$ of $CaCO_3$ (e.g., calcite) is controlled by $\delta^{18}O$ and temperature of the water body in which calcite precipitates (Faure, 1998). The $\delta^{18}O_{calcite}$ values in closed lake systems, as in this study, principally reflect the $\delta^{18}O$ composition of the lake water, influenced by the average $\delta^{18}O$ composition of precipitation (rainfall) in the basin, and the amount of evaporation, especially in arid regions (Kelts and Talbot, 1990; Leng and Marshall, 2004). The effects of evaporation are also related to the residence time of the lake water (i.e., time between recharge intervals). Long residence times allow the effects of evaporation (preferential removal of ^{16}O from the water body) to intensify, resulting in progressive increase in $\delta^{18}O_{water}$. In contrast, frequent recharge episodes (shorter residence times) renew the lake water with meteoric water (relatively enriched in ^{16}O), resulting in lower $\delta^{18}O$ of the lake water and of any calcite precipitated from it. As a result, the effects of temperature-dependent isotopic fractionation on $\delta^{18}O$ of calcite precipitated in closed lakes are not as marked as they are in hydrologically open systems. Moreover, under arid and hot conditions, temperature effects on $\delta^{18}O_{calcite}$ are opposite to those of evaporation. Therefore, in closed lakes $\delta^{18}O_{calcite}$ values are not a direct record of temperature variations, rather they record the stronger influence of evaporation on $\delta^{18}O_{water}$ (López Blanco et al., 2016; Vázquez-Urbez et al., 2013).

Lacustrine carbonate $\delta^{13}C$ reflects a combined signal from diverse carbon sources to, and processes in, the lake water (Li and Ku, 1997; Leng and Marshall, 2004; Arp et al., 2005). The dissolved inorganic carbon (DIC) isotopic composition controls the resulting carbonate precipitate composition. The $\delta^{13}C$ of the DIC pool is mainly controlled by the inflowing water composition, the CO_2 exchange between the lake water and the atmosphere, and the CO_2 derived from the degradation of the organic matter (Kelts and Talbot, 1990; Leng and

Marshall, 2004). Karst weathering of catchment marine limestones is the basis of the DIC pool, and typically the DIC has a value close to 0‰ (Leng and Marshall, 2004). In this case study, drainage was from Pyrenean carbonates, but the precise isotopic composition of the DIC is unknown because of the variety of marine carbonate rocks that may have contributed to it, spanning from Triassic to Paleogene. The DIC $\delta^{13}C$ is then modulated by isotopic effects and exchange. In middle-low latitude lacustrine systems, soil derived CO_2 is a major source of ^{12}C that decreases both the $\delta^{13}C$ of the DIC and any $CaCO_3$ precipitating from it (Faure, 1998). Conversely, extensive equilibration between atmospheric CO_2 and lake water, evaporation, and photosynthetic CO_2-uptake in the water column all increase $\delta^{13}C$ values of the DIC and any $CaCO_3$ precipitating from it (Leng and Marshall, 2004).

Lake carbonates that show noticeable covariation of $\delta^{13}C$ and $\delta^{18}O$, as in the stromatolites studied herein, are considered to have formed in hydrologically closed conditions, with a strong evaporation effect (Talbot, 1990; Kelts and Talbot, 1990; Arp et al., 2005).

9. Discussion

The interpretation of stable isotope data in ancient samples is contingent on assumptions regarding water temperature and kinetic effects caused by potentially variable rates of calcite precipitation. In the following discussion we assume that isotopic variability is mostly a product of near-equilibrium conditions, although we accept that non-equilibrium effects could have contributed to some of the variation. This approach is constrained to some extent by our knowledge of modern tufa stromatolites in the River Piedra (Spain) where tufa precipitation rates are high (≈ 1.4 cm/yr; Arenas et al., 2014). Despite high tufa precipitation rates, the coherence between measured and calculated water temperatures from $\delta^{18}O_{calcite}$ vouch for calcite precipitation close to equilibrium in the modern tufa (Osácar et al., 2013, 2016).

In closed lake basins the effects of evaporation produce a larger magnitude shift in $\delta^{18}O_{calcite}$ than temperature fractionation (Kelts and Talbot, 1990; Leng and Marshall, 2004). Therefore, $\delta^{18}O_{calcite}$ of closed lake basins mostly reflects the P/E ratio, with temperature effects either obscured, smoothed or blurred. (López Blanco et al., 2016; Vázquez-Urbez et al., 2013). It is thus difficult to infer the isotopic signature of the drainage water entering the lake: the lower $\delta^{18}O_{calcite}$ values of freshwater sedimentary facies should be closest to a drainage/meteoric water composition albeit contingent on an unknown water temperature.

Variation in calcite precipitation rates can influence calcite $\delta^{13}C$ and $\delta^{18}O$ isotopic via disequilibrium effects (e.g., Tremaine et al., 2011; Kele et al., 2015). Generally, isotopic equilibrium is thought difficult to achieve when precipitation rates are high, but the issue is complex (DePaolo, 2011).

9.1. Long-term depositional environmental evolution

Stromatolites and laminated limestones in this study have the heaviest isotopic compositions consistent with the interpretation of Arenas et al. (1997) in which stromatolites and laminated facies developed during periods characterized by a longer residence time of the lake water and intense evaporation (i.e., low P/E ratio). Bioclastic and bioturbated limestones developed during less intense evaporation periods and more frequent water renewal leading to dilution and relative increase in lake level (i.e., high P/E ratio).

In succession VS, in unit T5 (Figs. 2 and 6), the facies evolution reflects an overall shallowing that is corroborated by changes in stable isotope composition through time. The shallowest conditions (lower $\delta^{13}C$ and $\delta^{18}O$) correspond to bioturbated facies displaying desiccation cracks, breccias and Fe-rich oxidized surfaces, reflecting periodic subaerial exposure. The stromatolites correspond with heavier isotope compositions (Fig. 6) indicating more saline conditions, followed by an upward trend toward lower $\delta^{13}C$ and $\delta^{18}O$ values consistent with developing freshwater conditions (massive and bioturbated facies). This passage to freshwater conditions implies a relative deepening (decrease in isotopic values for Lm) followed by a shallowing to more palustrine conditions (increase in isotopic values for Lb).

Facies evolution in succession SC, in unit T6 (Figs. 2 and 7), corresponds to a deepening process. It is supported by the sharp change from higher (positive) $\delta^{18}O$ values of the basal mudstones representing saline mud flats, to progressively lower $\delta^{18}O$ values of laminated limestones and stromatolite facies, reflecting flooding by meteoric sourced drainage water (Casanova and Hillaire-Marcel, 1992) culminating in the lowest values in the uppermost marls.

When isotopic data from stromatolites throughout the studied succession are compared (Fig. 12) it is clear that unit T5 and T6 stromatolites mostly have higher values than those from unit T7 (Fig. 12B). This result is consistent with both the interpretations of Arenas et al. (1997) and with evolution toward less saline lacustrine environments from unit T5 to T7 (Arenas and Pardo, 1999). This trend suggests a change toward more humid climate conditions and, in the case of unit T7, accompanying increase of alluvial distal deposits from the progradation of a northern fluvial system (Arenas et al., 1997).

The strong positive correlation between $\delta^{18}O$ and $\delta^{13}C$ in units T5 and T6 (Figs. 8 and 9) is consistent with a closed lake depositional context. $\delta^{18}O$ is controlled mostly by variation in P/E (cf., Talbot, 1990; Frantz et al., 2014; Jones et al., 2016; López-Blanco et al., 2016) while $\delta^{13}C$ is likely recording the effects of water-atmosphere CO_2-exchange and of biological-derived ^{12}C contributions (Leng and Marshall, 2004).

The negative correlation between unit T7 $\delta^{18}O$ and $\delta^{13}C$ (Fig. 10) suggests that this stromatolite formed in a lake with more frequent water renewal and shorter water residence time. This local setting was favored by an overall more humid climate as inferred from the lower isotope values (Fig. 12B) and the almost invariant $\delta^{18}O$ and $\delta^{13}C$ through unit T7 in the Sierra de Alcubierre (cf., Arenas et al., 1997). This more humid context is also recorded in other continental basins in Spain in deposits partly correlative with unit T7 (e.g., the upper unit in the Madrid Basin; Alonso-Zarza et al., 2004).

9.2 Short-term stromatolite evolution: environmental and temporal significance of lamination

9.2.1 Coupling texture and isotopic composition of stromatolite lamination

$\delta^{18}O$ and $\delta^{13}C$ show similar relationships with texture at all orders of lamination (Figs. 11 and 13), an association that links stromatolite development with parameters that influence the stable isotope composition, mostly variations in the P/E ratio for the $\delta^{18}O$, and the varying sources of C and in-lake processes for the $\delta^{13}C$. This relation is also recognized on a number of temporal scales.

Textural features of the stromatolite are essentially similar in all morphological types, both spatially and temporally (Fig. 5). The principal driver for alternating dark and light laminae is microbial growth and presence of extracellular polymeric substances (EPS) participating in calcite precipitation as a response to climatic changes or their climate-related parameters (Andrews and Brasier, 2005; Decho et al., 2005; Nehza et al., 2009; Petryshyn et al., 2012) rather than microbial filament orientation or varying microbial groups (Tang et al., 2014). The influence of microbial activity and concomitant mineral precipitation on the textural differences between light and dark laminae (e.g., porosity and colour) is thus also linked to environmental and climate-related parameters, such as water temperature, hydrochemistry, hydraulics, and light intensity, which affect surface and subsurface metabolic activities of the microbial mats (Arp et al., 2010; Manzo et al., 2012; Dupraz et al., 2006, 2009). Ultimately, variations in these parameters cause or induce changes in mineral saturation levels in the water and therefore on textural features (see below).

In units T5 and T6, $\delta^{13}C_{calcite}$ and $\delta^{18}O_{calcite}$ show similar cyclicity at all scales, higher values coincident with the dark laminae and lower values with light laminae. $\delta^{18}O_{calcite}$ values in closed-lake systems mostly reflect the P/E ratio (e.g., Zamarreño et al., 1997; López-Blanco et al., 2016; Lettéron et al., 2018), whereas any temperature dependent fractionation effects on $\delta^{18}O_{calcite}$ signature are variably blurred (Leng and Marshall, 2004). Accordingly, the light, either

dense or porous, laminae, with lower $\delta^{18}O$ values, probably correspond to more humid conditions, while the dark dense laminae, with higher $\delta^{18}O$ values, represent drier conditions. Assuming climatic conditions similar to present-day in the area, the more evaporative conditions occurred during summer, while the humid conditions took place during spring and autumn (Fig. 13A, B). Despite the isotopic signature of the porous and dense laminae being opposite in hydrologically open and hydrologically closed depositional systems, the corresponding textural features are correlative (cf., Matsuoka et al., 2001). In fluvial stromatolites the porous laminae represent cooler or winter calcification and the dense laminae warmer calcification (Pentecost and Riding, 1986; Andrews and Brasier, 2005; Arenas and Jones, 2017). The textural features of the laminae are compatible with the greater density of the dark laminae being related to the higher levels of calcite saturation in lake waters reached during periods of low P/E ratio (i.e., during the warm and dry conditions). The effects of varying calcite saturation in the water from which the carbonate forms, on the sedimentary texture of carbonates precipitated, have been studied in modern and recent deposits, and variations are explained by the precipitation rates (Kano et al., 2007; Golubic, 2008). Commonly, high calcite precipitation rate yields denser fabrics formed of smaller crystals (Janssen et al., 1999; Gradzinski, 2010; Arenas and Jones, 2017). The intense degassing of CO_2 in warmer arid periods results in high pH and alkalinity, and consequently fast carbonate precipitation (Dupraz et al., 2009; Arp et al., 2010). Similar fabric effects have been described from several modern and recent stromatolites of fluvial tufa systems (Chafetz et al., 1991; Janssen et al., 1999; Gradzinski, 2010; Manzo et al., 2012; Arenas and Jones, 2017). Therefore, variations in the magnitude of water parameters such as temperature, Ca^{2+} and HCO_3^- concentration, and CO_2 content, which affect the calcite saturation levels of water, are likely drivers of textural variations between laminae.

During the driest, warmest months, increased water temperatures will impart a temperature-fractionation on $\delta^{18}O_{calcite}$ of opposite sign to that caused by evaporation, resulting in a reduction in the difference between $\delta^{18}O_{calcite}$ values of the corresponding seasonal deposits. This is consistent with the narrow $\delta^{18}O_{calcite}$ range between the dark and light laminae in the T5 and T6 stromatolites (Table 2). Assuming, under isotopic equilibrium conditions, a decrease of 0.24‰ in calcite $\delta^{18}O$ results from a 1ºC increase in water temperature (Craig, 1965), the mean equilibrium water temperature difference between the humid and dry periods would be between 1.6 to 4.0 ºC (based on mean calcite $\delta^{18}O$ of light and dark laminae). In unit T5, the difference would be ≈ 3ºC, in unit T6 ≈ 1.9ºC and in unit T7 ≈ 3ºC. We note that these differences are much smaller than seasonal water temperature differences observed in modern saline lakes 50–60 km SE of the study area (River Ebro Depression) where winter

temperatures are between 0.9–10.2ºC (December 2004) and between 19–35.3ºC in May 2005 (Casamayor et al., 2013; see also Hamer et al., 2007). These small differences suggest that our stromatolite record is underestimating the actual temperature, supporting the notion that temperature change was not the main control on $\delta^{18}O$: P/E ratio was.

The higher $\delta^{13}C$ values in the dark laminae of units T5 and T6, and the HRS variations, are most likely related to longer water residence time, allowing more time for exchange between atmospheric CO_2 and DIC, and also the photosynthetic assimilation of $^{12}CO_2$. Both processes promote increased $\delta^{13}C$ of DIC in the water (Leng and Marshall, 2004; Nehza et al., 2009). The lower $\delta^{13}C$ values in the light laminae may reflect higher input of soil-derived ^{12}C (e.g., Pentecost and Riding, 1986; Arp et al., 2005; Kano et al., 2007; Nehza et al., 2009), compatible with more humid conditions and cooler temperatures relative to the dark laminae. The overall lower $\delta^{13}C$ and $\delta^{18}O$ in unit T7 stromatolites indicate overall more humid conditions, with $\delta^{13}C$ indicating a larger contribution of soil-derived CO_2 and likely less intense exchange between atmospheric CO_2 and DIC (cf., Leng and Marshall, 2004; Andrews, 2005).

HRS cyclicity in $\delta^{18}O_{calcite}$ (Fig. 11) is also interpreted as a P/E ratio signal seen at a range of temporal scales (Fig. 13B, C). The three clear 1st order cycles with evolutions toward higher values have a mean difference of ~1‰ $\delta^{18}O_{calcite}$ from base to top. The gradual increase in $\delta^{18}O_{calcite}$ through each of these three cycles and the general $\delta^{18}O_{calcite}$ increase of the entire HRS record suggests stepped climate change towards drier conditions, likely indicative of an overall lake level decrease or "shallowing cycle". Similar, but shorter environmental variations may be recorded by the 2nd order cycles. Nehza et al. (2009) interpreted isotopic changes in 2nd order cycles of Cretaceous lacustrine stromatolites to indicate hydrological changes in the lake water, affecting both paleoproductivity and paleosalinity.

Sharp isotopic change at most boundaries between light and dark laminae at the 1st and 2nd frequencies, especially those at the top of dark laminae (Fig. 11B), could be related to the rapid decrease or even cessation in calcite precipitation (Brasier et al., 2010). The causes of these breaks could be associated with drastic drops of water level or even temperature decrease, i.e., precluding calcite precipitation (Arp et al., 2001). In most 2nd order cycles, the isotopic change coincides with the textural boundary, which is consistent with small hiatuses, as described by Nehza et al. (2009) and Brasier et al. (2010). However, at the 1st-order scale, the change in isotopic trend in some cycles is below the textural change, which may be due to more gradual changes in calcite precipitation rates (e.g., Dabkowski et al., 2015), without sedimentary interruption.

9.2.2 Temporal significance of the stromatolite lamination

The period(s) of time represented by stromatolite lamination is uncertain because of the variety of processes involved in their development and the varied arrangement of the laminae (Petryshyn et al., 2012; Arenas and Jones, 2017). The most common lamination pattern is alternation between light porous and dark dense laminae (Casanova, 1994; Brasier et al., 2010; Frantz et al., 2014). In a continental context, variations in temperature, precipitation and evaporation may cause this alternation (Chafetz et al., 1991; Lindqvist, 1994; Andrews and Brasier, 2005; Kano et al., 2007; Brasier et al., 2010; Solari et al., 2010; Frantz et al., 2014; Dabkowski et al., 2015). Eocene stromatolites in the Gosiute Paleolake of the Green River Formation (Rife Bed, Tipton Member) show seasonal lamination (Frantz et al., 2014) with fan microfabric forming during cooler periods, and micrite microfabrics when the lake was shallow and warm.

The formation of stromatolite laminae in spring-tufa deposits and marine systems are considered daily (Golubic and Focke, 1978; Vanyo and Awramik, 1982), seasonal or annual (Kano et al., 2007; Gradzinski, 2010) based on the textural and geochemical data. This noted, pluriannual laminae in Walker Lake Holocene stromatolites are proved by radiometric ages (Petryshyn et al., 2012). Modern fluvial stromatolites show that each pair of simple laminae can form in less than a few months, with periodic and non-periodic parameters influencing the lamina formation (Jones, 1981; Gradzinski, 2010; Arenas and Jones, 2017).

The textural and geochemical analyses of the Miocene lacustrine stromatolites in the Ebro Basin suggest two persistent orders of cyclicity that represent periodic changes of climate parameters, i.e. the P/E ratio. Given the persistent cyclicity, it is proposed that the composite laminae correspond to pluriannual periods of dominantly drier or more humid conditions. In this interpretation each couplet formed of a dark dense simple lamina (1 to 6 samples in the HRS) and a light porous or light dense simple lamina, would represent an annual period.

Integrating all the information, we suggest the light dense simple laminae developed during the rainy seasons (e.g., autumn and early spring) with recharging water introducing isotopically negative soil-organics and meteoric water, and favouring the formation of scattered allochems (ooids, intraclasts, bioclasts). The light porous simple laminae formed during spring-early summer with a faster microbial growth caused by increased nutrient supply, higher temperatures and illumination (Fig. 13A). The dark dense laminae developed mostly in the summer and perhaps early autumn, as evaporation and temperature increased, and soil-derived ^{12}C input decreased, leading to increased $\delta^{13}C_{calcite}$ and $\delta^{18}O_{calcite}$. During winter, temperature and light levels decreased, perhaps causing cessation of microbial growth (Pentecost, 1978; Arp et al., 2010). The succession of light dense, light porous and dark dense simple laminae thus corresponds to an annual period.

The light or dark composite laminae in stromatolites were thus controlled by variations in environmental and climatic conditions acting during longer periods (each of several years). Dark composite laminae might correspond to pluriannual drier conditions, while light composite laminae could represent pluriannual humid periods. Each 1st order cycle would represent longer pluriannual evolution to drier conditions. According to these tentative time estimates, the isotopic trends in the studied specimens represent centennial or millennial evolutionary trends of the lake level controlled by the P/E ratio.

10. Conclusions

Sedimentological and isotopic analyses ($\delta^{13}C$ and $\delta^{18}O$) of Early to Middle Miocene stromatolites from the Ebro Basin show:

1. That $\delta^{13}C$ and $\delta^{18}O$ compositions through ≈ 2 metre-thick facies successions confirm that the heavier isotope composition of stromatolites and muddy-grainy laminated limestones are due to higher evaporation/exchange and suggest a longer residence time of lake waters. The lakes were saline at this time and extensive isotopic exchange occurred between lake water DIC and atmospheric CO_2.
2. Textural and isotopic variations are coupled in the stromatolite lamination. The cyclic isotopic variation in successive dark and light composite laminae in five stromatolite specimens suggest that dark laminae developed during drier conditions while the light laminae developed during more humid conditions.
3. $\delta^{13}C$ and $\delta^{18}O$ records from high resolution sampling across a 2.1 cm-thick stromatolite section distinguish three orders of cyclic variation:
    - 3rd order cycles, recorded by the simple laminae, possibly formed by seasonal P/E variations.
    - 2nd order cycles represented by the dark and light composite laminae; each reflects, respectively, dominantly low and high P/E conditions during several years.
    - 1st order cycles formed by the succession of a light and a dark composite lamina, with increasing-upward isotopic values, reflecting lake level shallowing due to a decrease in the P/E ratio.

Acknowledgments

This work was funded by CGL2013-42867-P project and FPI contract BES-2014-069389 of the Spanish Government and European Regional Funds. The Optical Microscopy and Rock Preparation services of the University of Zaragoza, Spain (*Servicios de Apoyo a la Investigación*)

and Complutense University of Madrid are thanked for technical support. Prof. Paul Dennis (UEA), Prof. Robin Renaut (UEA) and Prof. Cinta Osácar (Unizar) are thanked for their advice. Dr. A. Sáez and other anonymous reviewers helped improve the quality of this contribution.

References

Abell, P.I., Awramik, S., Osborne, R.H., Tomellini, S., 1982. Plio-Pleistocene lacustrine stromatolites from lake Turkana, Kenya: morphology, stratigraphy and stable isotopes. Sediment. Geol. 32, 1-26. https://doi.org/10.1016/0037-0738(82)90011-2.

Adachi, N., Asada, Y., Ezaky, Y., Liu, J., 2017. Stromatolites near the Permian-Triassic boundary in Chongyang, Hubei Province, South China: A geobiological window into palaeo-oceanic fluctuations following the end-Permian Extinction. Palaeogeogr. Palaeoclimatol. Palaeoecol. 475, 55-69.

Alonso-Zarza, A.M., Calvo, J.P., Silvia P.G., Torres, T., 2004. Cuenca del Tajo, in: Vera, J.A.(Ed.), Geología de España. SGE-IGME, Madrid, pp. 556–561.

Andrews, J.E., Brasier, A.T., 2005. Seasonal records of climatic change in annually laminated tufas: Short review and future prospects. J. Quat. Sci. 20, 411–421. https://doi.org/10.1002/jqs.942.

Andrews, J.E., Riding, R., Dennis, P.F., 1993. Stable isotopic composition of Recent freshwater cyanobacterial carbonates from the British Isles; local and regional envrionmental control. Sedimentology 40(2), 303–314.

Arenas, C., 1993. Sedimentología y paleogeografía del Terciario del margen pirenaico y sector central de la Cuenca del Ebro (zona aragonesa occidental). PhD thesis. University of Zaragoza, Zaragoza. https://zaguan.unizar.es/record/70725.

Arenas, C., Auqué, L., Osácar, C., Sancho, C., Lozano, M.V., Vázquez-Urbez, M., Pardo, G., 2015. Current tufa sedimentation in a high discharge river: A comparison with other synchronous tufa records in the Iberian Range (Spain). Sediment. Geol. 325, 132–157. https://doi.org/10.1016/j.sedgeo.2015.05.007.

Arenas, C., Casanova, J., Pardo, G., 1997. Stable isotope characterization of the Miocene lacustrine systems of Los Monegros (Ebro Basin, Spain): palaeogeographic and palaeoclimatic implications. Palaeogeogr. Palaeoclimatol. Palaeoecol. 128, 133–155.

Arenas, C., Jones, B., 2017. Temporal and environmental significance of microbial lamination: Insights from Recent fluvial stromatolites in the River Piedra, Spain. Sedimentology 64, 1597–1629. https://doi.org/10.1111/sed.12365.

Arenas, C., Pardo, G., 1999. Latest Oligocene-Late Miocene lacustrine systems of the north-central part of the Ebro Basin (Spain): Sedimentary facies model and palaeogeographic

synthesis. Palaeogeogr. Palaeoclimatol. Palaeoecol. 151, 127–148. https://doi.org/10.1016/S0031-0182(99)00025-5.

Arenas, C., Vázquez-Ubez, M., Auqué, L., Sancho, C., Osácar, C. Pardo, G., 2014. Intrinsic and extrinsic controls of spatial and temporal variations in modern fluvial tufa sedimentation: A thirteen-year record from a semi-arid environment . Sedimentology 61, 90-132. https://doi.org/10.1111/sed.12045.

Arp, G., Bielert, F., Hoffmann, V.E., Löffler, T., 2005. Palaeoenvironmental significance of lacustrine stromatolites of the Arnstadt Formation ("Steinmergelkeuper", Upper Triassic, N-Germany). Facies 51, 419–441. https://doi.org/10.1007/s10347-005-0063-8.

Arp, G., Bissett, A., Brinkmann, N., Cousin, S., De Beer, D., Friedl, T., Mohr, K.I., Neu, T.R., Reimer, A., Shiraishi, F., Stackebrandt, E., Zippel, B., 2010. Tufa-forming biofilms of German karstwater streams: microorganisms, exopolymers, hydrochemistry and calcification. Geol. Soc. London, Spec. Publ. 336, 83–118. https://doi.org/10.1144/SP336.6.

Arp, G., Wedemeyer, N., Reitner, J., 2001. Fluvial tufa formation in a hard-water creek (Deinschwanger Bach, Franconian Alb, Germany). Facies 44, 1–22. https://doi.org/10.1007/BF02668163.

Beukes, N.J., Lowe, D., R., 1989. Environmental control on diverse stromatolite morphologies in the 3000 Myr Pongola Supergroup, South Africa. Sedimentology 36, 383–397. https://doi.org/10.1111/j.1365-3091.1989.tb00615.x.

Brasier, A.T., Andrews, J.E., Marca-Bell, A.D., Dennis, P.F., 2010. Depositional continuity of seasonally laminated tufas: Implications for $\delta^{18}O$ based palaeotemperatures. Glob. Planet. Change 71, 160–167. https://doi.org/10.1016/j.gloplacha.2009.03.022.

Casanova, J., Hillaire-Marcel, C., 1992. Chronology and paleohydrology of late Quaternary high lake levels in the Manyara basin (Tanzania) from isotopic data (18O, 13C, 14C, Th U) on fossil stromatolites. Quat. Res. 38, 205–226. https://doi.org/10.1016/0033-5894(92)90057-P.

Casanova, J., 1994. Stromatolites from the East African Rift: a synopsis, in: J. Bertrand-Sarfati and C. Monty (Eds), Phanerozoic Stromatolites II, Kluwer Academic Publishers, Dordrecht, The Netherlands, pp. 193–226.

Casamayor, E., Triadó-margarit, X., Castañeda, C., 2013. Microbial biodiversityin saline shallow lakes of the Monegros Desert, Spain. FEMS Microbial Ecol., 85, 503–518. https://doi.org/10.1111/1574-6941.12139.

Chafetz, H.S., Utech, N.M., Fitzmaurice, S.P., 1991. Differences in the $\delta^{18}O$ and $\delta^{13}C$ signatures of seasonal laminae comprising travertine stromatolites. J. Sediment. Petrol. 61, 1015–

1028.

Craig, H., 1965. The measurement of oxygen isotope palaeotempera- tures, in: Tongiorgi, E. (Ed.), Stable Isotopes in Oceanographic Studies and Palaeotemperatures. Consiglio Nazionale Della Richerche. Laboratorio de Geologia Nucleare, Pisa, pp. 161–182

Dabkowski, J., Royle, S.H., Antoine, P., Marca-Bell, A., Andrews, J.E., 2015. High-resolution $\delta^{18}O$ seasonality record in a French Eemian tufa stromatolite (Caours, Somme Basin). Palaeogeogr. Palaeoclimatol. Palaeoecol. 438, 277–284. https://doi.org/10.1016/j.palaeo.2015.08.017.

Decho, A.W., Visscher, P.T., Reid, R.P., 2005. Production and cycling of natural microbial exopolymers (EPS) within a marine stromatolite. Palaeogeogr. Palaeoclimatol. Palaeoecol. 219, 71–86. https://doi.org/10.1016/j.palaeo.2004.10.015.

DePaolo, D.J., 2011. Surface kinetic model for isotopic and trace element fractionation during precipitation of calcite from aqueous solutions. Geochim. Cosmochim. Acta 75, 1039–1056.

Dupraz, C., Pattisina, R., Verrecchia, E.P., 2006. Translation of energy into morphology: Simulation of stromatolite morphospace using a stochastic model. Sed. Geol., 185, 185–203.

Dupraz, C., Reid, R.P., Braissant, O., Decho, A.W., Norman, R.S., Visscher, P.T., 2009. Processes of carbonate precipitation in modern microbial mats. Earth-Sci. Rev. 96, 141–162. https://doi.org/10.1016/j.earscirev.2008.10.005.

Faure, G. 1998. Principles and Applications of Geochemistry. Prentice Hall, Inc. New Jerey, USA.

Frank, T.D., Lyons, T.W., Lohmann, K.C., 1997. Isotopic evidence for the paleoenvironmental evolution of the mesoproterozoic Helena formation, belt supergroup, Montana, USA. Geochim. Cosmochim. Acta 61, 5023–5041. https://doi.org/10.1016/S0016-7037(97)80341-9.

Frantz, C.M., Petryshyn, V.A., Marenco, P.J., Tripati, A., Berelson, W.M., Corsetti, F.A., 2014. Dramatic local environmental change during the Early Eocene Climatic Optimum detected using high resolution chemical analyses of Green River Formation stromatolites. Palaeogeogr. Palaeoclimatol. Palaeoecol. 405, 1–15. https://doi.org/10.1016/j.palaeo.2014.04.001.

Golubic, S., Violante, C., Plenkovic-Moraj, A., Grgasovic, T., 2008. Travertines and calcareous tufa deposits: an insight into diagenesis. Geol. Croat. 61, 363–378.

Golubic, S., Focke, J.W., 1978. Phormidium hendersoni Howe: Identity and significanca of a modern stromatolite building microorganisms. J. Sed. Pet. 48, 751–764.

Gradzinski, M., 2010. Factors controlling growth of modern tufa: results of a field experiment. Geol. Soc. London, Spec. Publ. 336, 143–191. https://doi.org/10.1144/SP336.8.

Grotzinger, J.P., Knoll, A.H., 1999. Stromatolites in Precambrian carbonates: evolutionary mileposts or environmental dipsticks? Annu. Rev. Earth Planet. Sci. 27, 313–358. https://doi.org/10.1146/annurev.earth.27.1.313.

Hamer, J.M.M., Sheldon, N.D., Nichols, G.J., Collinson, M.E., 2007. Late Oligocene-Early Miocene paleosols of distal fluvial systems, Ebro Basin, Spain. Palaeogeogr. Palaeoclimatol. Palaeoecol. 247, 220–235. https://doi.org/10.1016/j.palaeo.2006.10.016.

Janssen, A., Swennen, R., Podoor, N., Keppens, E., 1999. Biological and diagenetic influence in recent and fossil tufa deposits from Belgium. Sed. Geol. 126, 75–95. https://doi.org/10.1016/S0037-0738(99)00033-0.

Jones, C., 1981. Periodicities in stromatolite lamination from the Early Proterozoic Hearne Formation, Great Slave lake, Canada. Palaeontology 24, 231–250.

Jones, M.D., Cuthbert, M.O., Leng, M.J., McGowan, S., Mariethoz, G., Arrowsmith, C., Sloane, H.J., Humphrey, K.K., Cross, I., 2016. Comparisons of observed and modelled lake $\delta^{18}O$ variability. Quat. Sci. Rev. 131, 329–340. https://doi.org/10.1016/j.quascirev.2015.09.012.

Kano, A., Hagiwara, R., Kawai, T., Hori, M., Matsuoka, J., 2007. Climatic conditions and hydrological change recorded in a high-resolution stable-isotope profile of a recent laminated tufa on a subtropical island, southern Japan. J. Sediment. Res. 77, 59–67. https://doi.org/10.2110/jsr.2007.006.

Kele, S., Breitenbach, S.F.M., Capezzuoli, E., Meckler, A.N., Ziegler, M., Millan, I.M., Kluge, T., Deák, J., Hanselmann, K., John, C.M., Yan, H., Liu, Z., Bernasconi, S.M., 2015. Temperature dependence of oxygen- and clumped isotope fractionation in carbonates: a study of travertines and tufas in the 6–95 °C temperature range. Geochim. Cosmochim. Acta 168, 172–192. https://doi.org/10.1016/j.gca.2015.06.032.

Kelts, K., Talbot, M.R., 1990. Lacustrine carbonates as geochemical archives of environmental change and Biotic/Abiotic Interactions, in: Tilzer, M.M., Serruya, C. (Eds.), Large Lakes. Springer-Verlag, Berlin, pp. 288–315.

Leng, M.J., Marshall, J.D., 2004. Palaeoclimate interpretation of stable isotope data from lake sediment archives. Quat. Sci. Rev. 23, 811–831. https://doi.org/10.1016/j.quascirev.2003.06.012.

Lettéron, A., Hamon, Y., Fournier, F., Séranne, M., Pellenard, P., Joseph, P., 2018. Reconstruction of a saline, lacustrine carbonate system (Priabonian, St-Chaptes Basin, SE France): Depositional models, paleogeographic and paleoclimatic implications. Sediment.

Geol. 367, 20–47. https://doi.org/10.1016/j.sedgeo.2017.12.023.

Li, H.C., Ku, T.L., 1997. $\delta^{13}C$–$\delta^{18}O$ covariance as a paleohydro- logical indicator for closed-basin lakes. Palaeogeogr. Palaeoclimatol. Palaeoecol. 133, 69–80.

Lindqvist, J.K., 1994. Lacustrine stromatolites and oncoids. Manuherikia Group (Miocene), New Zealand, in: Bertrand-Sarfati, J., Monty, C. (Eds.), Phanerozoic Stromatolites II. Kluwer Academic Publishers, Dordrecht, pp. 227–254.

López-Blanco, C., Andrews, J., Dennis, P., Rosa, M., Vicente, E., 2016. North Atlantic Oscillation recorded in carbonate $\delta^{18}O$ signature from Lagunillo del Tejo (Spain). Palaeogeogr. Palaeoclimatol. Palaeoecol. 441, 882–889. https://doi.org/10.1016/j.palaeo.2015.10.037.

Manzo, E., Perri, E., Tucker, M.E., 2012. Carbonate deposition in a fluvial tufa system: processes and products (Corvino Valley – southern Italy). Sedimentology 59, 553–577.

Martin-Bello, L., Arenas, C., Jones, B., 2019. Lacustrine stromatolites: Useful structures for environmental interpretation – an example from the Miocene Ebro Basin. Sedimentology. https://doi.org/10.1111/sed.12577.

Matsuoka, J., Kano, A., Oba, T., Watanabe, T., Sakai, S., Seto, K., 2001. Seasonal variation of stable isotopic compositions recorded in a laminated tufa, SW Japan. Earth Planet. Sci. Lett. 192, 31–44. https://doi.org/10.1016/S0012-821X(01)00435-6.

Monty, C.L.V., 1967. The origin and development of cryptalgal fabrics, in: Walter, M.R. (Ed.), Stromatolites. Elsevier, Amsterdam, pp. 193–249.

Muñoz, A., Arenas, C., González, A., Luzón, A., Pardo, G., Pérez, A., Villena, J., 2002. Ebro Basin (Northeastern Spain), in: Gibbons, W., Moreno, T. (Eds.), The Geology of Spain. Geological Society, London, pp. 301–309.

Nehza, O., Woo, K.S., Lee, K.C., 2009. Combined textural and stable isotopic data as proxies for the mid-Cretaceous paleoclimate: A case study of lacustrine stromatolites in the Gyeongsang Basin, SE Korea. Sediment. Geol. 214, 85–99. https://doi.org/10.1016/j.sedgeo.2008.03.012.

Oliveri, E.O., Neri, R., Bellanca, A., Riding, R., 2010. Carbonate stromatolites from a Messinian hypersaline setting in the Caltanissetta Basin , Sicily: petrographic evidence of microbial activity and related stable isotope and rare earth element signatures. Sedimentology 57, 142–161. https://doi.org/10.1111/j.1365-3091.2009.01094.x.

Osácar, M.C., Arenas, C., Auqué, L., Sancho, C., Pardo, G., Vázquez-Urbez, M., 2016. Discerning the interactions between environmental parameters reflected in $\delta^{13}C$ and $\delta^{18}O$ of recent fluvial tufas: Lessons from a Mediterranean climate region. Sediment. Geol. 345, 126–144. https://doi.org/10.1016/j.sedgeo.2016.09.004.

Osácar, M.C., Arenas, C., Sancho, C.S., Pardo, G., Martín Bello, L., 2017. Stable-isotope changes

in tufa stromatolites of the Quaternary Añamaza fluvial system (Iberian Ranges, Spain). Geogaceta 61, 167–170.

Osácar, M.C., Arenas, C., Vazquez-Urbez, M., Sancho, C., Auque, L.F., Pardo, G., 2013. Environmental Factors Controlling the $\delta^{13}C$ and $\delta^{18}O$ Variations of Recent Fluvial Tufas: A 12-Year Record from the Monasterio de Piedra Natural Park (NE Iberian Peninsula). J. Sediment. Res. 83, 309–322. https://doi.org/10.2110/jsr.2013.27.

Pardo, G., Arenas, C., González, A., Luzón, A., Muñoz, A., Pérez, A., Pérez-Rivarés, F.J., Vázquez-Úrbez, M., Villena, J., 2004. La Cuenca del Ebro, in: Vera, J.A. (Ed.), Geología de España. SGE-IGME, Madrid, pp. 533–543.

Park, R., 1976. A note on the significance of lamination in stromatolites. Sedimentology 23, 379–393.

Pentecost, A., Riding, R., 1986. Calcification in cyanobacteria, in: Leadbeater, B.S.C., Riding, R. (Eds.), Biomineralisation in Lower Plants and Animals. Syst. Assoc. Spec. Publ., pp. 73–90.

Pérez Rivarés, F.J., 2016. Estudio magnetoestratigráfico del Mioceno del sector central de la Cuenca del Ebro: Cronología, correlación y análisis de la ciclicidad sedimentaria. Ph.D. thesis, University of Zaragoza, Zaragoza.

Pérez-Rivarés, F.J., Arenas, C., Pardo, G., Garcés, M., 2018. Temporal aspects of genetic stratigraphic units in continental sedimentary basins: Examples from the Ebro basin, Spain. Earth-Science Rev. 178, 136–153. https://doi.org/10.1016/j.earscirev.2018.01.019.

Petryshyn, V.A., Corsetti, F.A., Berelson, W.M., Beaumont, W., Lund, S.P., 2012. Stromatolite lamination frequency, Walker Lake, Nevada: Implications for stromatolites as biosignatures. Geology, 40, 499–502. https://doi.org/10.1130/G32675.1.

Reid, R.P., James, N.P., Macintyre, I.G., Dupraz, C.P., Burne, R. V., 2003. Shark Bay Stromatolites : Microfabrics and Reinterpretation of Origins. Facies 49, 299–324. https://doi.org/10.1007/s10347-003-0036-8.

Riba, O., Reguant, S., Villena, J., 1983. Ensayo de síntesis estratigáfica y evolutiva de la cuenca terciaria del Ebro, in: Comba, J.A. (Ed.), Geología de España, Libro Jubilar J.M. Ríos. Instituto Geológico y Minero de España, Madrid, pp. 131–159.

Riding, R., 2000. Microbial carbonates: the geological record of calcified bacterial-algal mats and biofilms. Sedimentology 47, 179–214. https://doi.org/10.1046/j.1365-3091.2000.00003.x.

Rodríguez-Berriguete, Á., Alonso-Zarza, A.M., Martín-García, R., Cabrera, M. del C., 2018. Sedimentology and geochemistry of a human-induced tufa deposit: Implications for palaeoclimatic research. Sedimentology, 65(7), 2253–2277. https://doi.org/10.1111/sed.12464.

Sanz-Montero, M.E., Rodríguez-Aranda, J.P., García Del Cura, M.A., 2008. Dolomite-silica stromatolites in miocene lacustrine deposits from the Duero Basin, spain: The role of organotemplates in the precipitation of dolomite. Sedimentology 55, 729–750. https://doi.org/10.1111/j.1365-3091.2007.00919.x.

Solari, M.A., Hervé, F., Le Roux, J.P., Airo, A., Sial, A.N., 2010. Paleoclimatic significance of lacustrine microbialites: A stable isotope case study of two lakes at Torres del Paine, southern Chile. Palaeogeogr. Palaeoclimatol. Palaeoecol. 297, 70–82. https://doi.org/10.1016/j.palaeo.2010.07.016.

Talbot, M.R., 1990. A review of the palaeohydrological interpretation of carbon and oxygen isotopic ratios in primary lacustrine carbonates. Chem. Geol. Isot. Geosci. Sect. 80, 261–279. https://doi.org/10.1016/0168-9622(90)90009-2.

Talbot, M.R., Kelts, K., 1990. Palaeolimnological signatures from carbon and oxygen isotopic ratios in carbonates from organic carbon-rich lacustrine sediments, in: Katz, B. (Ed.), Lacustrine Basin Exploration: Case Studies and Modern Analogs. Am. Assoc. Pet. Geol. Mem., Tusla, 50, pp. 99–112.

Tang, D., Shi, X., Jiang, G., 2014. Sunspot cycles recorded in Mesoproterozoic carbonate biolaminites. Precambrian Res. 248, 1–16. https://doi.org/10.1016/j.precamres.2014.04.009.

Tremaine, D.M., Froelich, P.N., Wang, Y., 2011. Speleothem calcite farmed in situ:modern calibration of δ^{18}Oand δ^{13}C paleoclimate proxies in a continuously-monitored natural cave system. Geochim. Cosmochim. Acta 75, 4929–4950. https://doi.org/ 10.1016/j.gca.2011.06.005.

Vanyo, J.P., Awramik, S.M., 1982. Length of day and obliquity of the ecliptic 850 MA ago: Preliminary results of a stromatolite growth model. Geophys. Res. Lett. 9, 1125–1128. https://doi.org/10.1029/GL009i010p01125.

Vasconcelos, C., McKenzie, J.A., Warthmann, R., Bernasconi, S.M., 2005. Calibration of the δ^{18}O paleothermometer for dolomite precipitated in microbial cultures and natural environments. Geology 33, 317–320. https://doi.org/10.1130/G20992.1.

Vazquez-Urbez, M., Arenas, C., Pardo, G., Perez-Rivares, J., 2013. The Effect of Drainage Reorganization and Climate On the Sedimentologic Evolution of Intermontane Lake Systems: The Final Fill Stage of the Tertiary Ebro Basin (Spain). J. Sed. Res. 83, 562–590. https://doi.org/10.2110/jsr.2013.47

Walter, M.R., 1972. Stromatolites and the biostratigraphy of the Australian Precambrian and Cambrian. Palaeontol. Asoc. Spec. Pub. 11, 256.

Zamarreño, I., Anadón, P., Utrilla, R. 1997. Sedimentology and isotopic composition of Upper

Palaeocene to Eocene non-marine stromatolites, eastern Ebro Basin, NE Spain. Sedimentology, 44, 159–176.

Captions of figures and tables

Figure 1. A) Location of the Ebro Basin in the northeast of the Iberian Peninsula. B) Study area Sierra de Alcubierre and tectosedimentary units T5, T6 and T7 of the Miocene (Arenas and Pardo, 1999). Ages of the units are (Pérez Rivarés et al., 2018): T5 between 20.8 ± 0.66 Ma and 16.2 ± 0.14 Ma (C5Cn.2n and C5Cn.1), T6 between 16.2 ± 0.14 Ma and 14.3 ± 0.14 Ma (C5ADn) and T7 begun 14.3 ± 0.14 Ma ago and spanned to C5ABn (13.608 to 13.363 Ma). The location of the sampled sections is indicated by a red line for Valle de Soler (VS), Puig Ladron (PL), San Caprasio (SC) and Aldea del correo (AC).

Figure 2. Four representative stratigraphic sections from the Sierra de Alcubierre (modified from Arenas, 1993). Stromatolite specimens VS-22, PL-22't, SC-141t, SC-197 and AC-9 were sampled for the isotopic analyses. Position of the facies associations shown in Figures 6 and 7 is also indicated.

Figure 3. Field views of the main facies in the Sierra de Alcubierre. A) Succession of marls (M), thin planar stromatolites (Ls. 1), laminar gypsum (Gl) and laminated limestones with parallel lamination (Ll.3). B) Succession of domed stromatolites (Ls.3) and laminated limestones with hummocky cross stratification (Ll.2). C) Succession of marls (M), thin planar stromatolites (Ls.1) and stratiform stromatolites (Ls.2). D) Laminated limestones with wavy stratification (Ll.1) and stromatolite fragments on top of bioturbated facies (Lb).

Figure 4. Two main facies associations distinguished in the Sierra de Alcubierre by Arenas and Pardo (1999). A) Deepening and shallowing processes. B) Shallowing process. Facies symbols in Table 1.

Figure 5. Textural variations between the different types of laminae. A) Composite alternating lamination; light porous and light dense alternation forming light composite laminae (LCL) and dark dense laminae with intercalated thinner light porous laminae forming dark composite laminae (DCL). B) Composite alternating lamination; porous laminae with thin dark dense intercalations (LCL) and the succession of dark dense laminae (DCL). C) Composite alternating lamination; dark composite laminae (DCL) alternating with porous simple laminae (LP). D) Simple alternating lamination between dark dense and light porous laminae. E) and F) Textural and color variations of the same sample, from thin section under petrographic optical microscope (E) and polished section under binocular microscope (F).

Figure 6. Facies succession VS from unit T5. A) Field view of bioturbated and laminated limestones of the upper part of the succession. B) Field view of marls, stromatolite and laminated limestones of the lower part of the succession. The hammer is 33 cm long. C) Detailed vertical facies succession from VS section. D) Stable isotopic data from the different facies of the facies succession. E) Water depth evolution inferred from sedimentary facies and stable isotope composition.

Figure 7. Facies succession SC from unit T6. A) Field view of the whole facies succession. The hammer is 33 cm long. B) Field view of stromatolite and laminated limestones of the lower part of the succession. C) Detailed vertical facies succession from San Caprasio section. D) Stable isotopic data from the different facies of the facies succession. E) Water depth evolution inferred from sedimentary facies and stable isotope composition.

Figure 8. Bulk sampling analyses from stromatolite specimens in unit T5. A) Cross section of specimen PL-22't (left panel) with sampling microboreholes and location of Figure 10B. Right panel shows stable isotope profile. B) Cross section of specimen VS-22 (left panel) with sampling microboreholes and stable isotope profile (right panel).

Figure 9. Bulk sampling analyses from stromatolite specimens in unit T6. A) Cross section of specimen AC-9 with sampling microboreholes and stable isotope profile. B) Cross section of specimen SC-141t with sampling microboreholes and stable isotope profile.

Figure 10. Bulk sampling analyses from stromatolite specimen in unit T7. Cross section of specimen SC-197b with sampling microboreholes and stable isotope profile.

Figure 11. High-resolution sampling (HRS) stable isotope data from a portion of stromatolite PL-22't (see Fig. 7A). A) Polished tablet for HRS with location of bulk analysis and the ranges of samples. B) HRS $\delta^{18}O$ and $\delta^{13}C$ analyses correlated with their position in the polished tablet. Three orders of cyclicity are indicated: first order cycles correspond to successive composite light and dark laminae with increasing stable isotope values; second order cycles correspond to each composite lamina; and third order cycles to each couple of single light and dark laminae.. At the top of two 1st order cycles, the $\delta^{18}O_{calcite}$ values are slightly lower than the highest isotopic values, located a few points below (n. 14 and 139). D) Bulk isotopic sampling analyses (see Fig. 7A) correlated with the HRS. Note that the bulk isotopic analysis are coincident with the corresponding mean values from HRS.

Figure 12. $\delta^{18}O$ and $\delta^{13}C$ plot: A) stromatolite facies in the different tectosedimentary units (T5, T6 and T7). B) different facies in the Sierra de Alcubierre compared data from Arenas et al. (1997).

Figure 13. A) Schematic of the environmental factors controlling the development of each lamina type. B) $\delta^{18}O$ and $\delta^{13}C$ ranges from high-resolution sampling (HRS) and corresponding textural variations in thin section with inferred temporal and climatic conditions. C) Lamina arrangement from thin section view of a stromatolite, with the three orders of cyclicity, typical relative variations of bulk and HRS isotopic composition based on the data in this paper, and the corresponding evolution of the P/E ratio.

Table 1. Sedimentary facies, their textural and structural features, and depositional interpretation in the Sierra de Alcubierre, summarized from Arenas et al. (1997). Stable isotope values ($\delta^{18}O$ and $\delta^{13}C$, ‰ VPDB) of the different facies (parenthesized values from Arenas et al., 1997).

Table 2. Mean values and ranges of stable isotope composition ($\delta^{18}O$ and $\delta^{13}C$, ‰ VPDB) of composite light and dark stromatolite laminae for each specimen (SC-197b, SC-141, AC-9, PL-22't and VS-22) in the three tectosedimentary units (T5, T6, and T7).

Table 1

Sedimentary facies	TSU	N.	Calcite $\delta^{13}C$ (‰ VPDB)	Calcite $\delta^{18}O$ (‰ VPDB)	Texture and components	Sedimentary structures	Interpretation
Bioturbated Limestones: Lb	5	4 (17)	–2.5 ± 0.9 (–3.1 ± 1.4)	–5.6 ± 0.6 (–6.1 ± 0.9)	Mudstones and wackestones. Gastropods, ostracods and charophytes	Bioturbation (root traces), desiccation cracks, nodules and breccias.	Palustrine conditions. Shallowing of previous fresh water ponded areas
Bioclastic massive limestones: Lm		3 (10)	–1.6 ± 0.2 (–2.6 ± 2.6)	–4.8 ± 3.3 (–6.1 ± 1.2)	Mudstones and wackestones. Gastropods, ostracods and charophytes	Massive, non-laminated. If present, weak bioturbation (root traces)	Freshwater, shallow lacustrine areas. Permanent water supply
Laminated Limestones: Ll Ll.1		18 (47)	–1.3 ± 0.7 (–1.9 ± 0.9)	–2.8 ± 2.0 (–2.9 ± 2.7)	Micrite and dolomicrite with mm to cm detrital laminae and lenses. Detritals include quartz, intraclasts, coated grains, ooids and bioclasts. Carbonate grains commonly form packstones and rare rudstones. Silicate grains constitute very fine to coarse sandstones	Lenticular or wavy stratification	Wave action during fair-weather conditions, above storm-surge level
Ll.2						Hummocky cross stratification	Dominant storm-surge action below fair-weather wave level
Ll.3						Parallel lamination	Shore sheet flows or inner turbidite-like currents offshore
Marls: M		4 (4)	–1.5 ± 1.3 (–3.0 ± 0.7)	–3.5 ± 3.3 (–4.6 ± 0.9)	Fine siliciclastic (clays and silts) sediment and lime mud. Gastropods, ostracods, charophytes and bioturbation	Structureless or with horizontal lamination or lenticular bedding	Settle-out of fine sediment in offshore lake areas in relation to water inputs
Stromatolitic Limestones: Ls Ls.1	5, 6 & 7	13 (59)	–2.7 ± 1.3 (–1.7 ± 1.2)	–4.7 ± 1.0 (–3.2 ± 2.6)	Boundstones. Lamination composed of simple laminae: dark dense micrite, light porous micrite to microsparite, and light dense micrite. Combined in composite dark and light laminae	Thin planar stromatolites	Microbial growth structures in shallow/marginal lacustrine areas. Moderate salinity waters and varying water depth and surge action
Ls.2						Stratiform stromatolite	
Ls.3						Domed stromatolite	
Oncolitic Limestones: Lo						Oncolites	
Mudstones: Fg, Fo					Green, grey and ochre. Siliciclastic sediment (clays and silts)	Structureless or parallel lamination	Nearshore lake areas or alluvial plains surrounding lacustrine areas. Locally deltaic deposits
Sandstones: Sm, Sr					Siliciclastic sand-size sediment	Massive, rippled and though-cross	Sheet flows and channels of alluvial plain near or within the

and St						stratification	lake areas.
Nodular gypsum: Gn					Alabastrine, saccharoid	Nodules, grouped in beds or isolated within other deposits	Evaporative processes in saline mud flats
Lenticular Gypsum: Glen					Alabastrine, saccharoid	Lenticular bedding and rarely forming laminae	Gypsum precipitation in water lake and interstitial within the sediment.
Rippled & Laminated Gypsum: Gr, Gl					Alabastrine, saccharoid	Parallel and rippled lamination, and lenticular bedding	Gypsum precipitation in hypersaline lake water.

Table 2
Mean values and ranges of stable isotope composition ($\delta^{18}O$ and $\delta^{13}C$, ‰ VPDB) of composite light and dark stromatolite laminae for each of the specimens (SC-197b, SC-141, AC-9, PL-22't and VS-22) in the three tectosedimentary units (T5, T6, and T7).

		Light laminae (‰ VPDB)				**Dark laminae** (‰ VPDB)						
Unit	Sample	$\delta^{13}C_{mean}$	$\delta^{13}C$-range	$\delta^{18}O_{mean}$	$\delta^{18}O$-range	$\delta^{13}C_{mean}$	$\delta^{13}C$-range	$\delta^{18}O_{mean}$	$\delta^{18}O$-range	Correl. Coeff.	**N**	**p** *value*
T7	SC-197b	–4.1	–4.7 to –3.7	–6.3	–7.1 to –4.9	–4.3	–4.6 to –4.0	–5.6	–6.5 to –5.0	–0.9	10	0.0005
T6	SC-141	–1.9	–2.0 to –1.6	–5.0	–5.4 to –4.4	–1.5	–1.8 to –1.3	–4.4	–4.8 to –4.1	+0.7	12	0.025
	AC-9	–1.2	–1.3 to –1.1	–4.2	–4.5 to –3.8	–1.0	–1.3 to –0.9	–3.8	–4.0 to –3.4	+0.5	19	0.01
T5	PL-22't	–0.9	–1.0 to –0.7	–5.1	–5.4 to –4.7	–0.5	–0.5 to –0.5	–4.1	–4.3 to –4.1	+0.9	11	0.0005
	VS-22	–1.4	–1.5 to –1.2	–3.9	–4.2 to –3.6	–1.0	–1.2 to –0.9	–3.4	–3.8 to –3.1	+0.5	30	0.0005

Highlights

1. Textural and isotopic variations are coupled in lacustrine stromatolite lamination
2. High-resolution sampling reflects three different orders of cyclicity
3. Lamination records seasonal to pluriannual precipitation/evaporation variations
4. Studied specimens represent centennial-millennial records of lake level variations

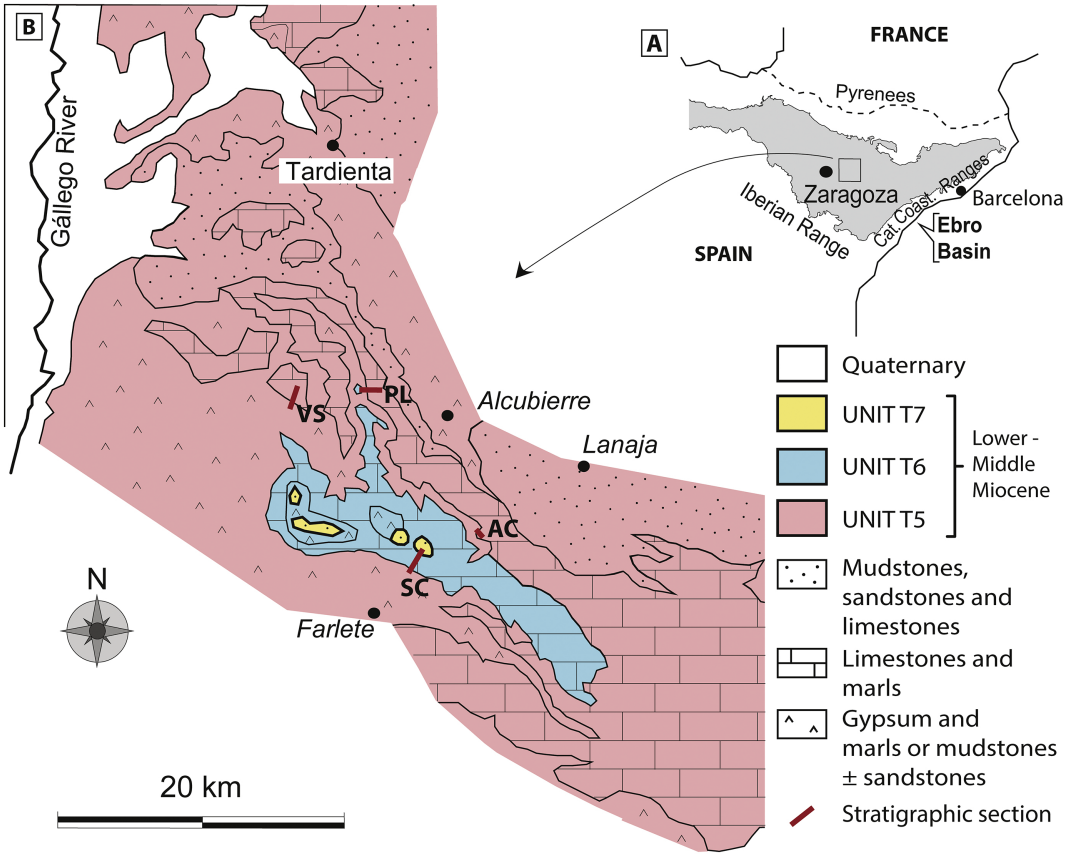
B
Gállego River
Tardienta
A
FRANCE
Pyrenees
Zaragoza
Barcelona
Iberian Range
Cat. Coast. Ranges
Ebro Basin
SPAIN
VS
PL
Alcubierre
Lanaja
AC
SC
Farlete
N
20 km
Quaternary
UNIT T7
UNIT T6
UNIT T5
Lower - Middle Miocene
Mudstones, sandstones and limestones
Limestones and marls
Gypsum and marls or mudstones ± sandstones
Stratigraphic section

Figure 1

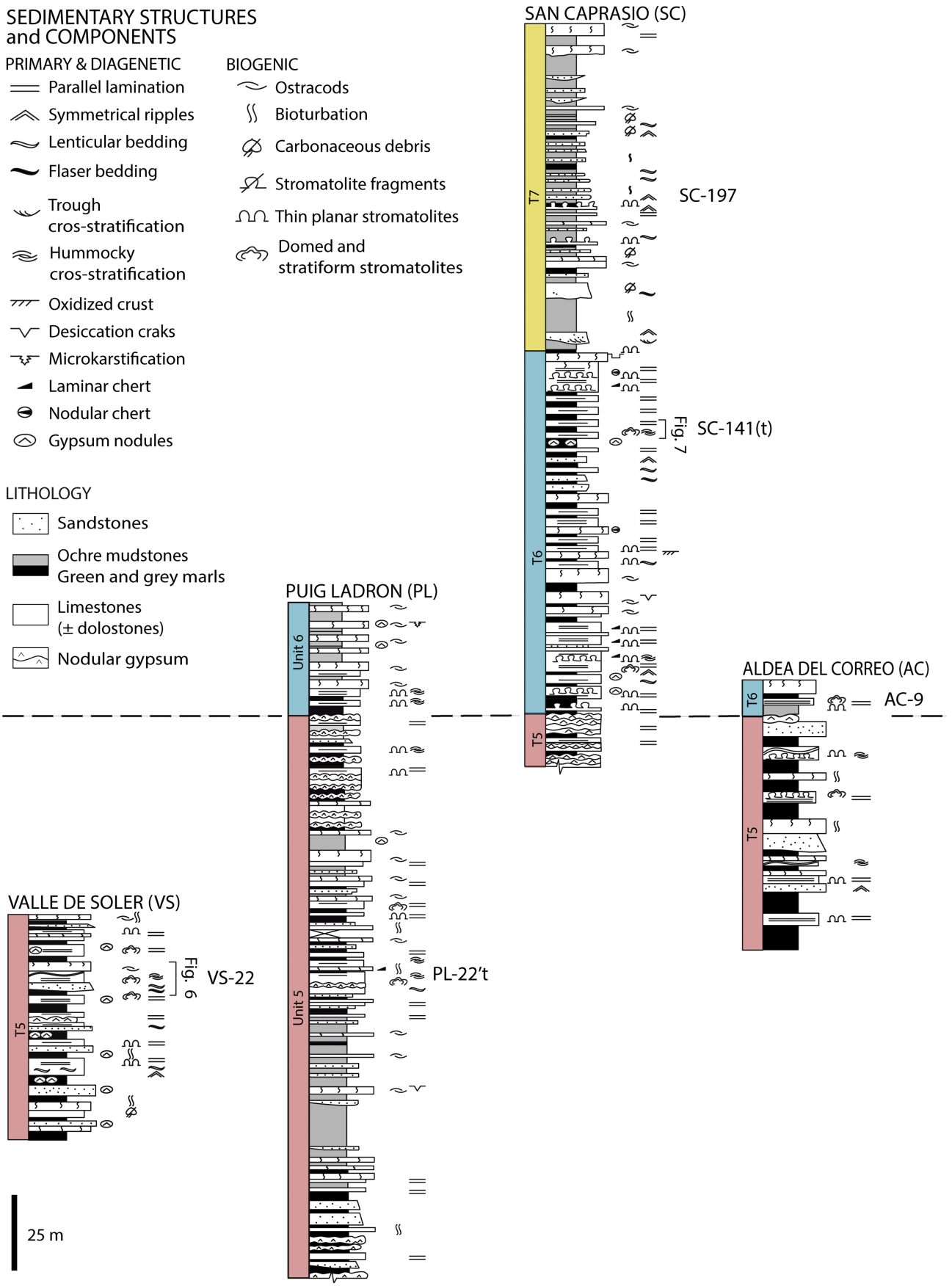
SEDIMENTARY STRUCTURES and COMPONENTS
PRIMARY & DIAGENETIC
Parallel lamination
Symmetrical ripples
Lenticular bedding
Flaser bedding
Trough cros-stratification
Hummocky cros-stratification
Oxidized crust
Desiccation craks
Microkarstification
Laminar chert
Nodular chert
Gypsum nodules
BIOGENIC
Ostracods
Bioturbation
Carbonaceous debris
Stromatolite fragments
Thin planar stromatolites
Domed and stratiform stromatolites
LITHOLOGY
Sandstones
Ochre mudstones
Green and grey marls
Limestones (± dolostones)
Nodular gypsum
SAN CAPRASIO (SC)
T7
T6
T5
SC-197
SC-141(t)
Fig. 7
PUIG LADRON (PL)
Unit 6
Unit 5
PL-22't
ALDEA DEL CORREO (AC)
T6
T5
AC-9
VALLE DE SOLER (VS)
T5
VS-22
Fig. 9
25 m

Figure 2

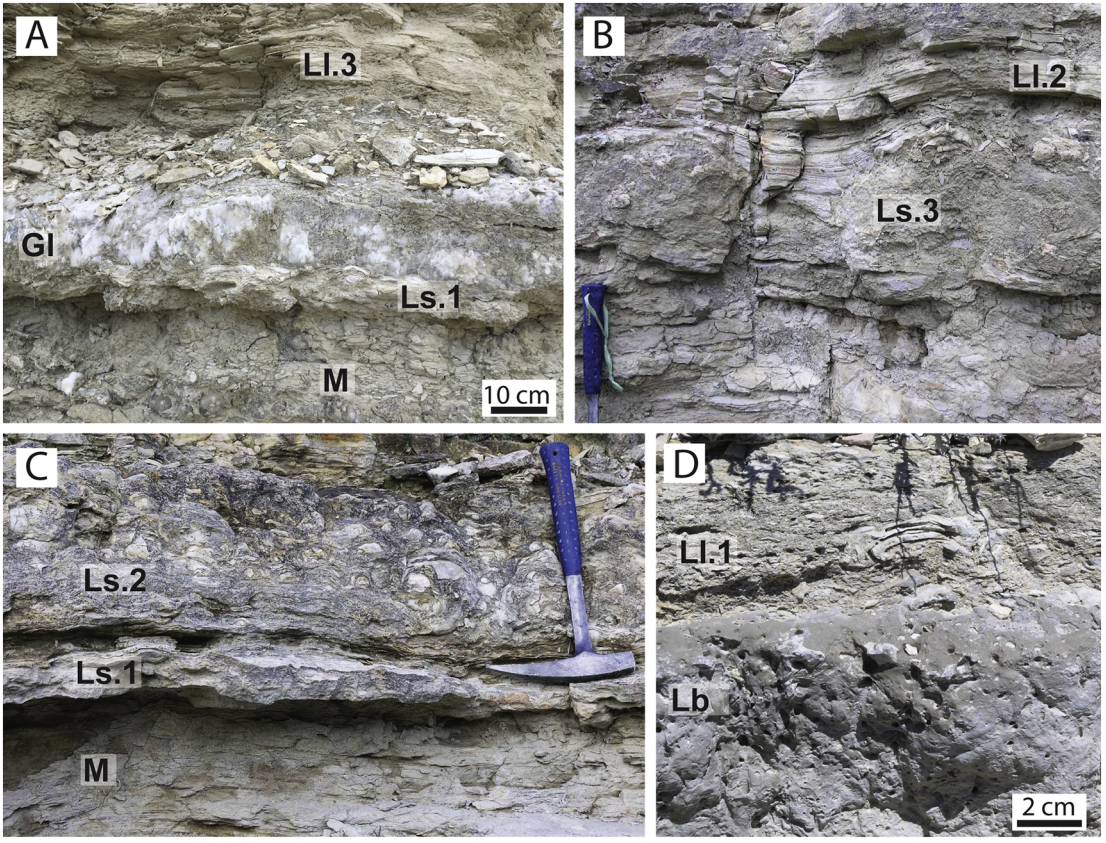

Figure 3

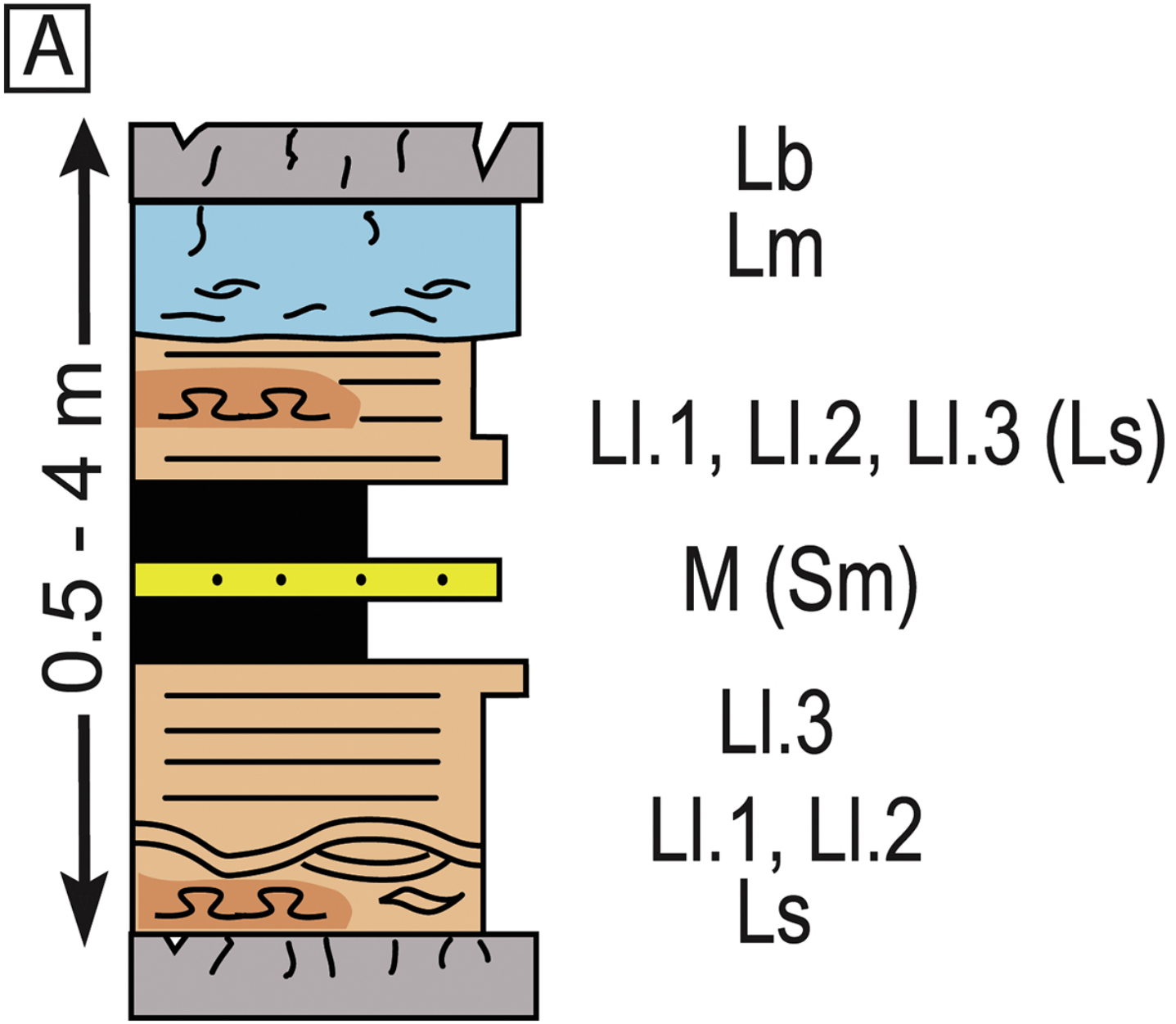

Figure 4

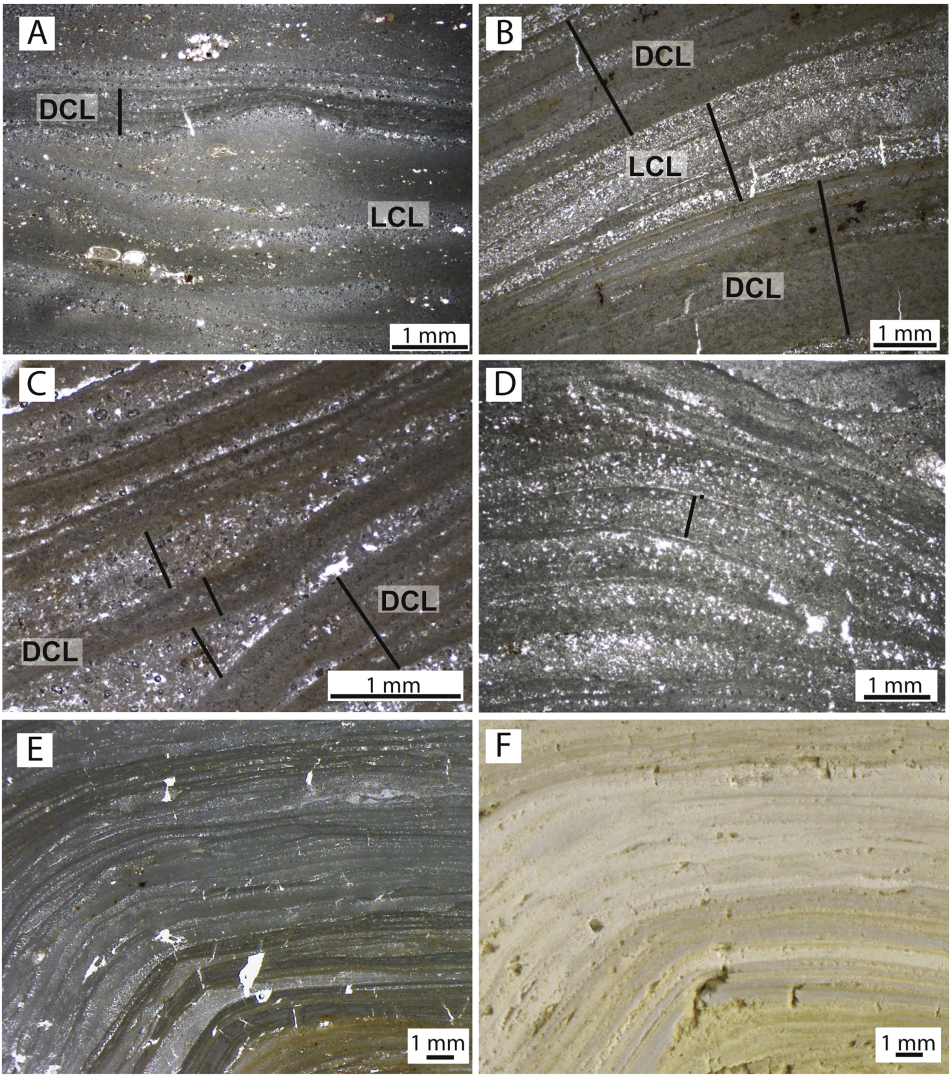

Figure 5

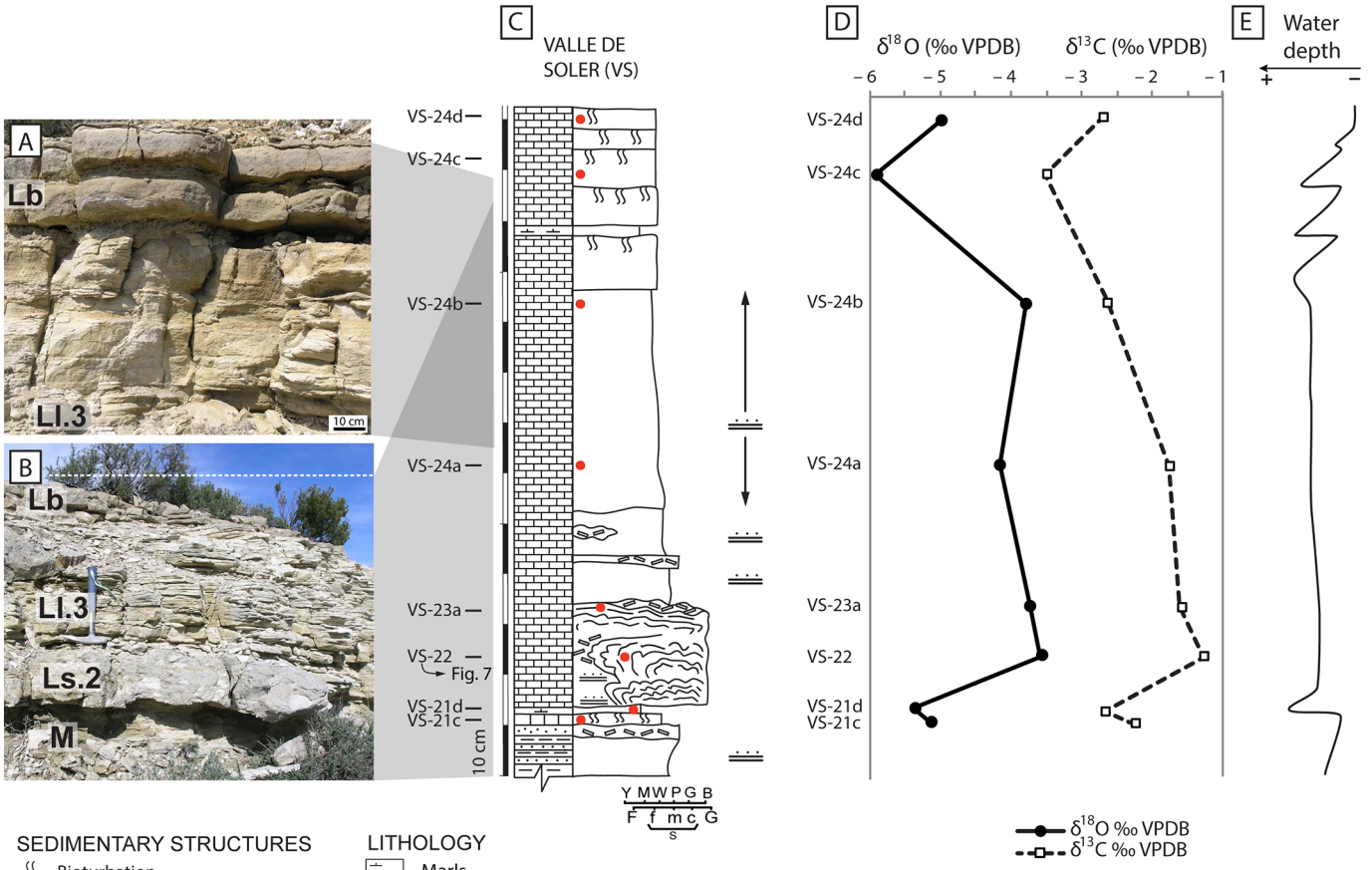
A
Lb
Ll.3
10 cm
B
Lb
Ll.3
Ls.2
M
C
VALLE DE SOLER (VS)
VS-24d
VS-24c
VS-24b
VS-24a
VS-23a
VS-22
Fig. 7
VS-21d
VS-21c
10 cm
Y M W P G B
F f m c s G
D
δ18O (‰ VPDB)
δ13C (‰ VPDB)
– 6 – 5 – 4 – 3 – 2 – 1
VS-24d
VS-24c
VS-24b
VS-24a
VS-23a
VS-22
VS-21d
VS-21c
E
Water depth
+ –
δ18O ‰ VPDB
δ13C ‰ VPDB
SEDIMENTARY STRUCTURES
Bioturbation
Stromatolite fragments
Carbonate-detritic parallel lamination
Sample location
LITHOLOGY
Marls
Sandstones
Green and grey mudstones
Limestones (± dolostones)

Figure 6

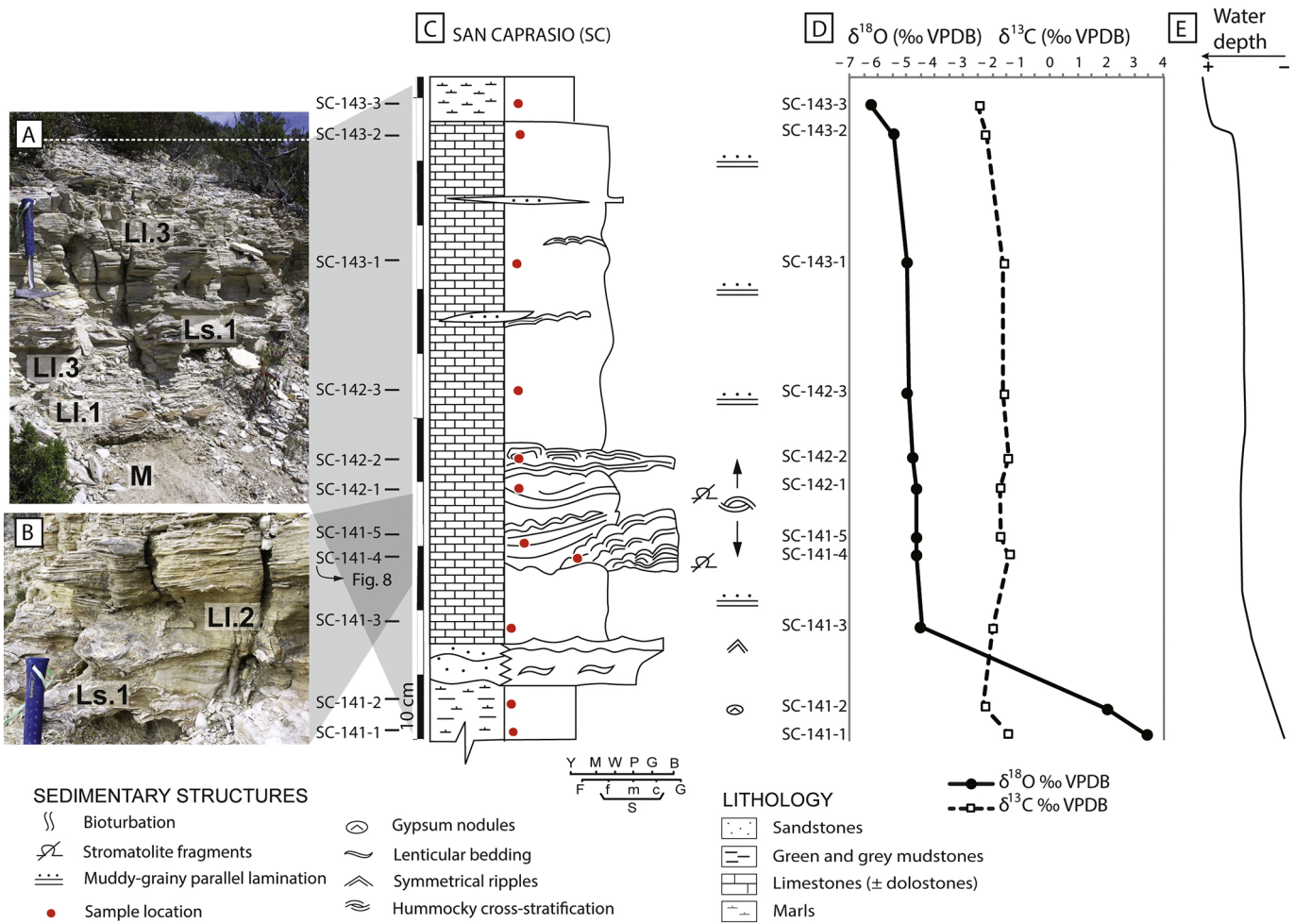
A
LI.3
Ls.1
LI.3
LI.1
M
B
LI.2
Ls.1
C SAN CAPRASIO (SC)
SC-143-3
SC-143-2
SC-143-1
SC-142-3
SC-142-2
SC-142-1
SC-141-5
SC-141-4
Fig. 8
SC-141-3
SC-141-2
SC-141-1
10 cm
Y M W P G B
F f m c G
S
D δ18O (‰ VPDB) δ13C (‰ VPDB)
−7 −6 −5 −4 −3 −2 −1 0 1 2 3 4
E Water depth
+ −
δ18O ‰ VPDB
δ13C ‰ VPDB
SEDIMENTARY STRUCTURES
Bioturbation
Stromatolite fragments
Muddy-grainy parallel lamination
Sample location
Gypsum nodules
Lenticular bedding
Symmetrical ripples
Hummocky cross-stratification
LITHOLOGY
Sandstones
Green and grey mudstones
Limestones (± dolostones)
Marls

Figure 7

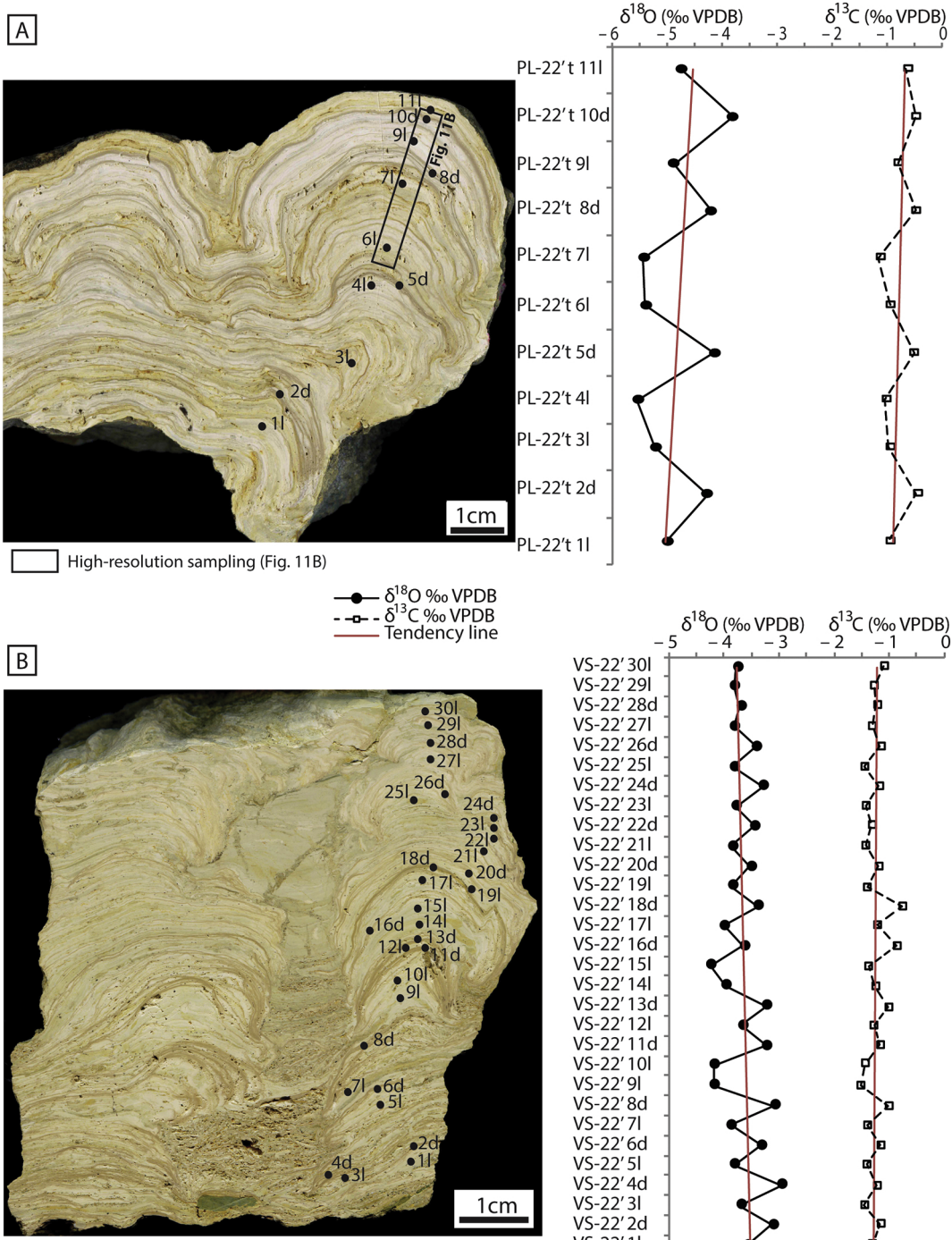
A
δ18O (‰ VPDB)
δ13C (‰ VPDB)
−6 −5 −4 −3 −2 −1 0
PL-22′t 11l
PL-22′t 10d
PL-22′t 9l
PL-22′t 8d
PL-22′t 7l
PL-22′t 6l
PL-22′t 5d
PL-22′t 4l
PL-22′t 3l
PL-22′t 2d
PL-22′t 1l
11l
10d
9l
Fig. 11B
8d
7l
6l
5d
4l
3l
2d
1l
1cm
High-resolution sampling (Fig. 11B)
δ18O ‰ VPDB
δ13C ‰ VPDB
Tendency line
B
δ18O (‰ VPDB)
δ13C (‰ VPDB)
−5 −4 −3 −2 −1 0
VS-22′30l
VS-22′29l
VS-22′28d
VS-22′27l
VS-22′26d
VS-22′25l
VS-22′24d
VS-22′23l
VS-22′22d
VS-22′21l
VS-22′20d
VS-22′19l
VS-22′18d
VS-22′17l
VS-22′16d
VS-22′15l
VS-22′14l
VS-22′13d
VS-22′12l
VS-22′11d
VS-22′10l
VS-22′9l
VS-22′8d
VS-22′7l
VS-22′6d
VS-22′5l
VS-22′4d
VS-22′3l
VS-22′2d
VS-22′1l
30l
29l
28d
27l
25l
26d
24d
23l
22l
21l
18d
20d
17l
19l
15l
16d
14l
13d
12l
11d
10l
9l
8d
7l
6d
5l
2d
1l
4d
3l
1cm

Figure 8

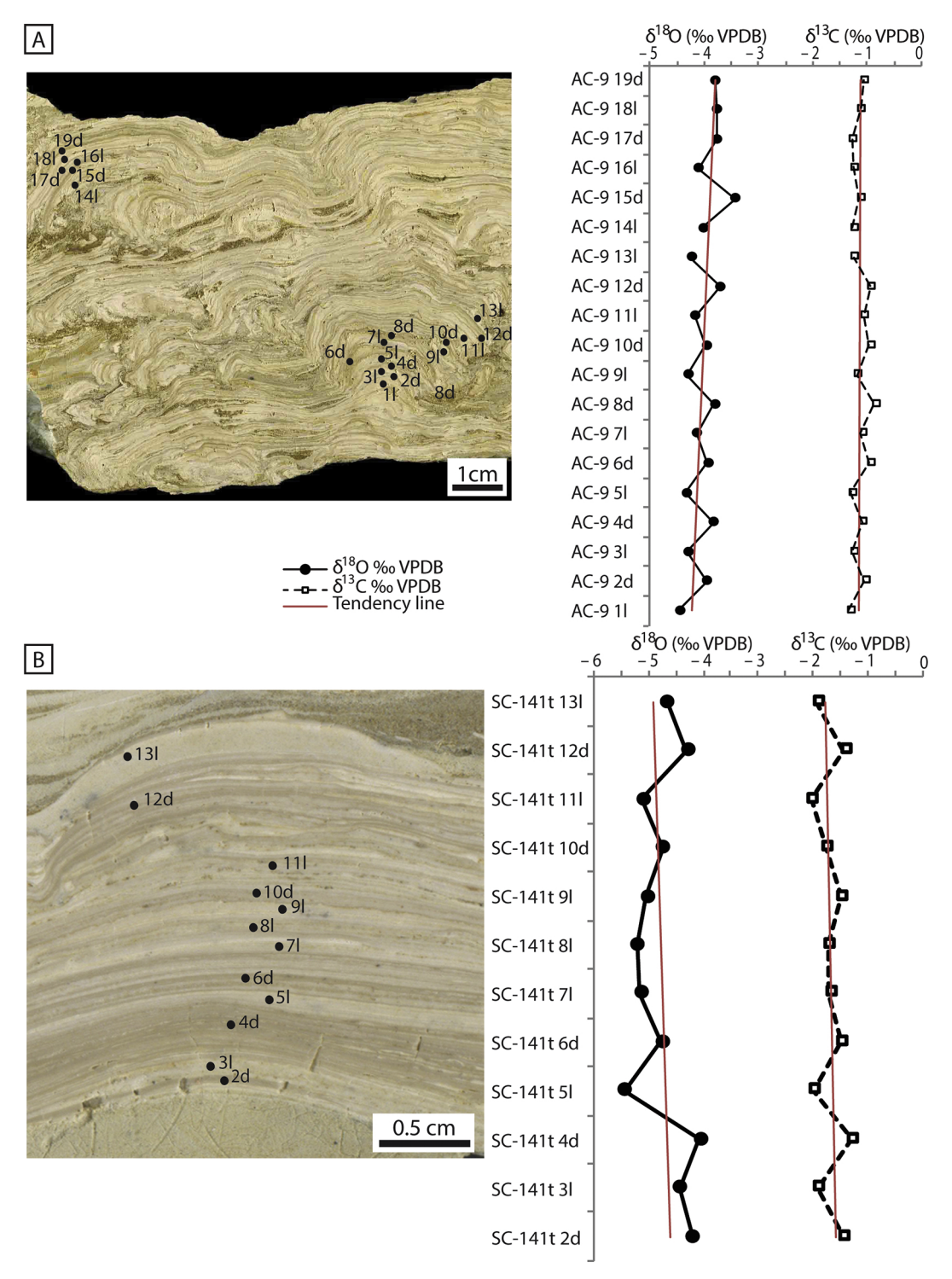
A
19d
18l
16l
17d
15d
14l
13l
8d
7l
10d
12d
6d
5l
9l
11l
4d
3l
2d
1l
8d
1cm
δ18O ‰ VPDB
δ13C ‰ VPDB
Tendency line
δ18O (‰ VPDB)
δ13C (‰ VPDB)
−5
−4
−3
−2
−1
0
AC-9 19d
AC-9 18l
AC-9 17d
AC-9 16l
AC-9 15d
AC-9 14l
AC-9 13l
AC-9 12d
AC-9 11l
AC-9 10d
AC-9 9l
AC-9 8d
AC-9 7l
AC-9 6d
AC-9 5l
AC-9 4d
AC-9 3l
AC-9 2d
AC-9 1l
B
13l
12d
11l
10d
9l
8l
7l
6d
5l
4d
3l
2d
0.5 cm
δ18O (‰ VPDB)
δ13C (‰ VPDB)
−6
−5
−4
−3
−2
−1
0
SC-141t 13l
SC-141t 12d
SC-141t 11l
SC-141t 10d
SC-141t 9l
SC-141t 8l
SC-141t 7l
SC-141t 6d
SC-141t 5l
SC-141t 4d
SC-141t 3l
SC-141t 2d

Figure 9

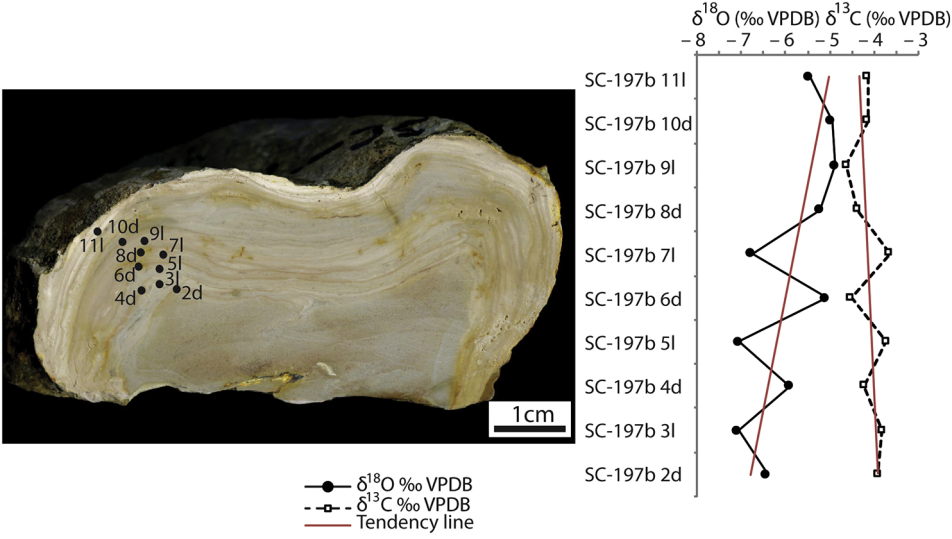
δ18O (‰ VPDB) δ13C (‰ VPDB)
−8 −7 −6 −5 −4 −3
SC-197b 11l
SC-197b 10d
SC-197b 9l
SC-197b 8d
SC-197b 7l
SC-197b 6d
SC-197b 5l
SC-197b 4d
SC-197b 3l
SC-197b 2d
11l
10d
9l
8d
7l
6d
5l
4d
3l
2d
1cm
δ18O ‰ VPDB
δ13C ‰ VPDB
Tendency line

Figure 10

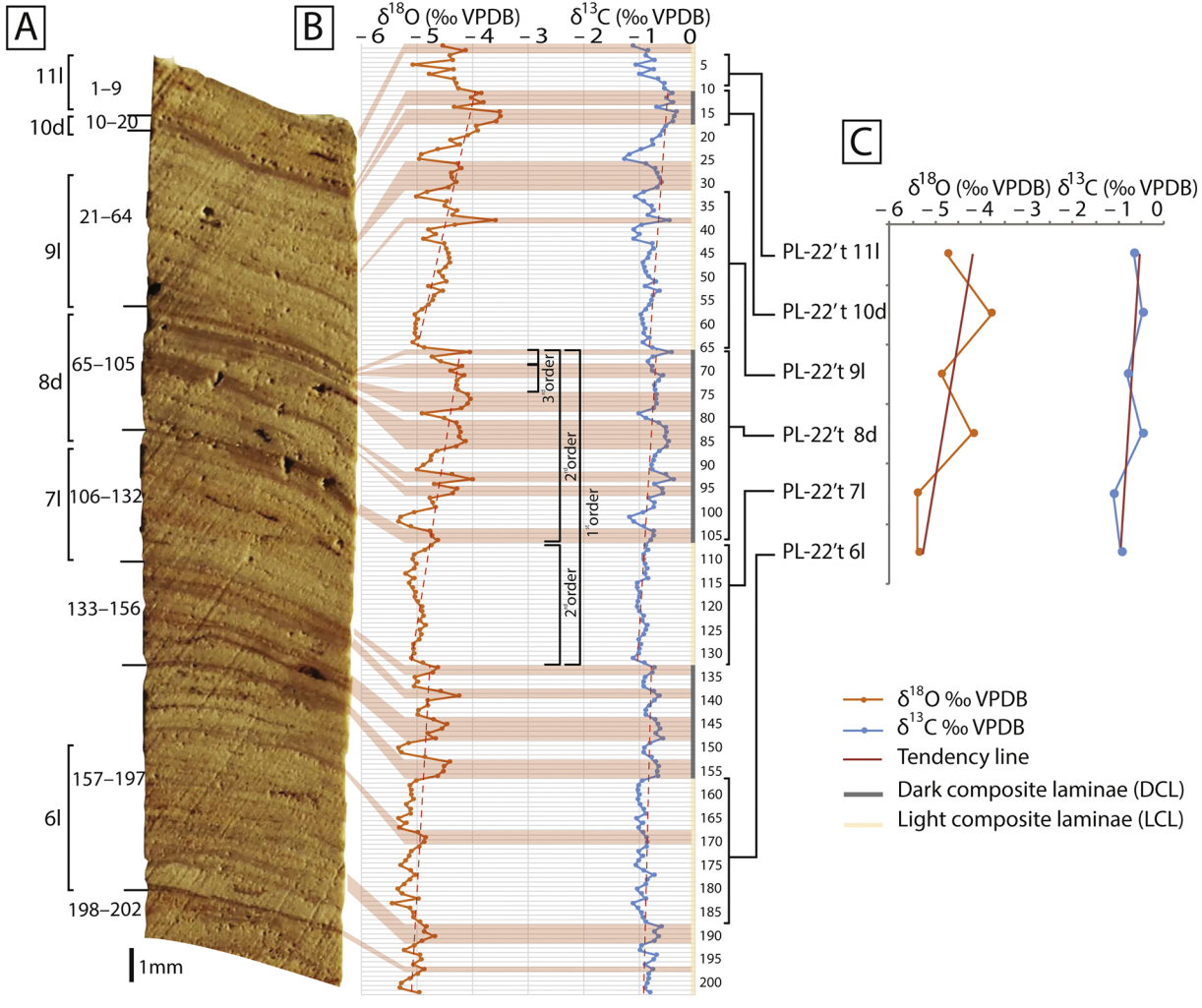
A
B
C
δ18O (‰ VPDB)
δ13C (‰ VPDB)
– 6 – 5 – 4 – 3 – 2 – 1 0
11l
10d
9l
8d
7l
6l
1–9
10–20
21–64
65–105
106–132
133–156
157–197
198–202
1mm
3°order
2°order
2°order
1°order
PL-22't 11l
PL-22't 10d
PL-22't 9l
PL-22't 8d
PL-22't 7l
PL-22't 6l
δ18O ‰ VPDB
δ13C ‰ VPDB
Tendency line
Dark composite laminae (DCL)
Light composite laminae (LCL)

Figure 11

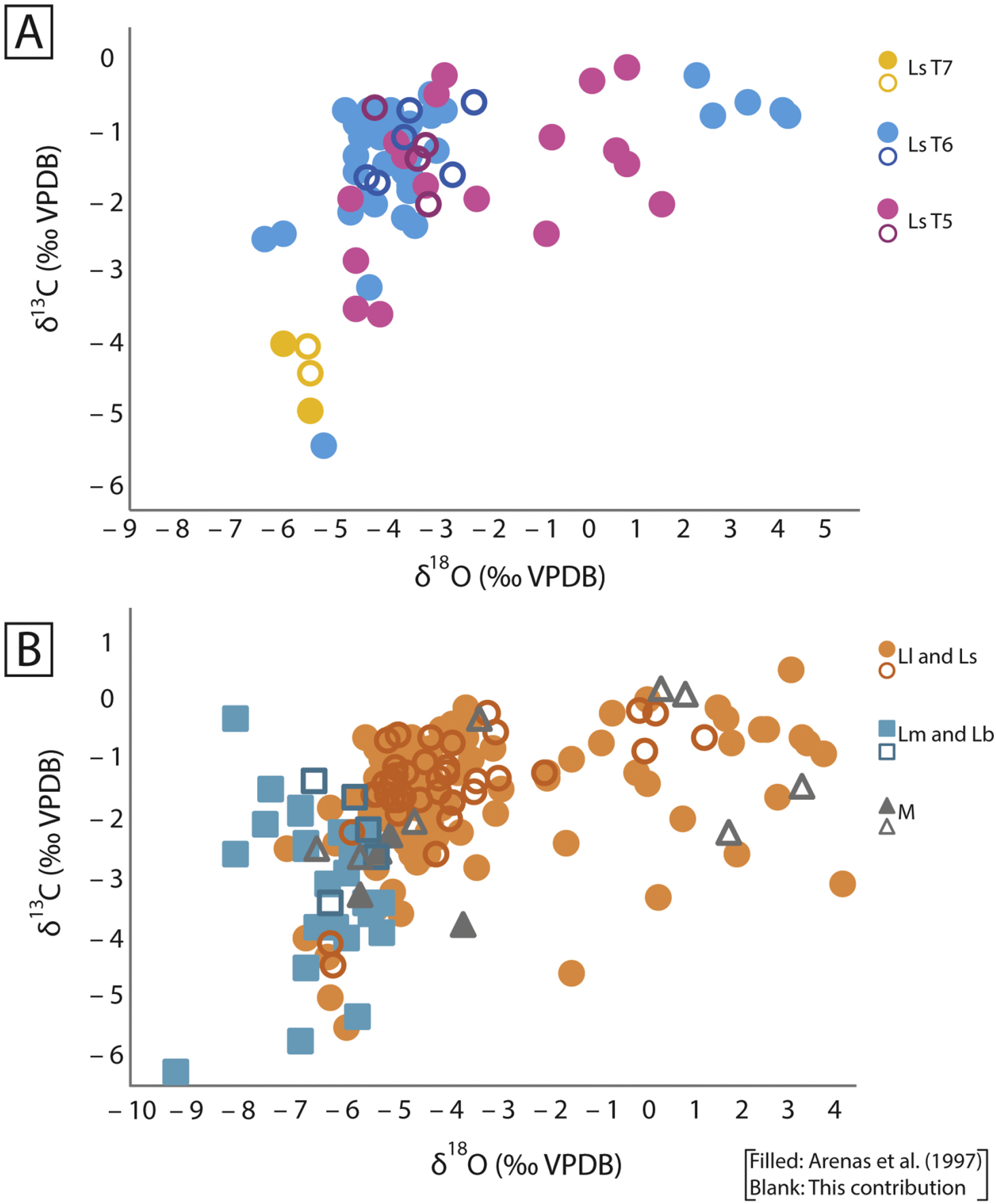
A
0
– 1
– 2
– 3
– 4
– 5
– 6
δ13C (‰ VPDB)
– 9 – 8 – 7 – 6 – 5 – 4 – 3 – 2 – 1 0 1 2 3 4 5
δ18O (‰ VPDB)
Ls T7
Ls T6
Ls T5
B
1
0
– 1
– 2
– 3
– 4
– 5
– 6
δ13C (‰ VPDB)
– 10 – 9 – 8 – 7 – 6 – 5 – 4 – 3 – 2 – 1 0 1 2 3 4
δ18O (‰ VPDB)
Ll and Ls
Lm and Lb
M
Filled: Arenas et al. (1997)
Blank: This contribution

Figure 12

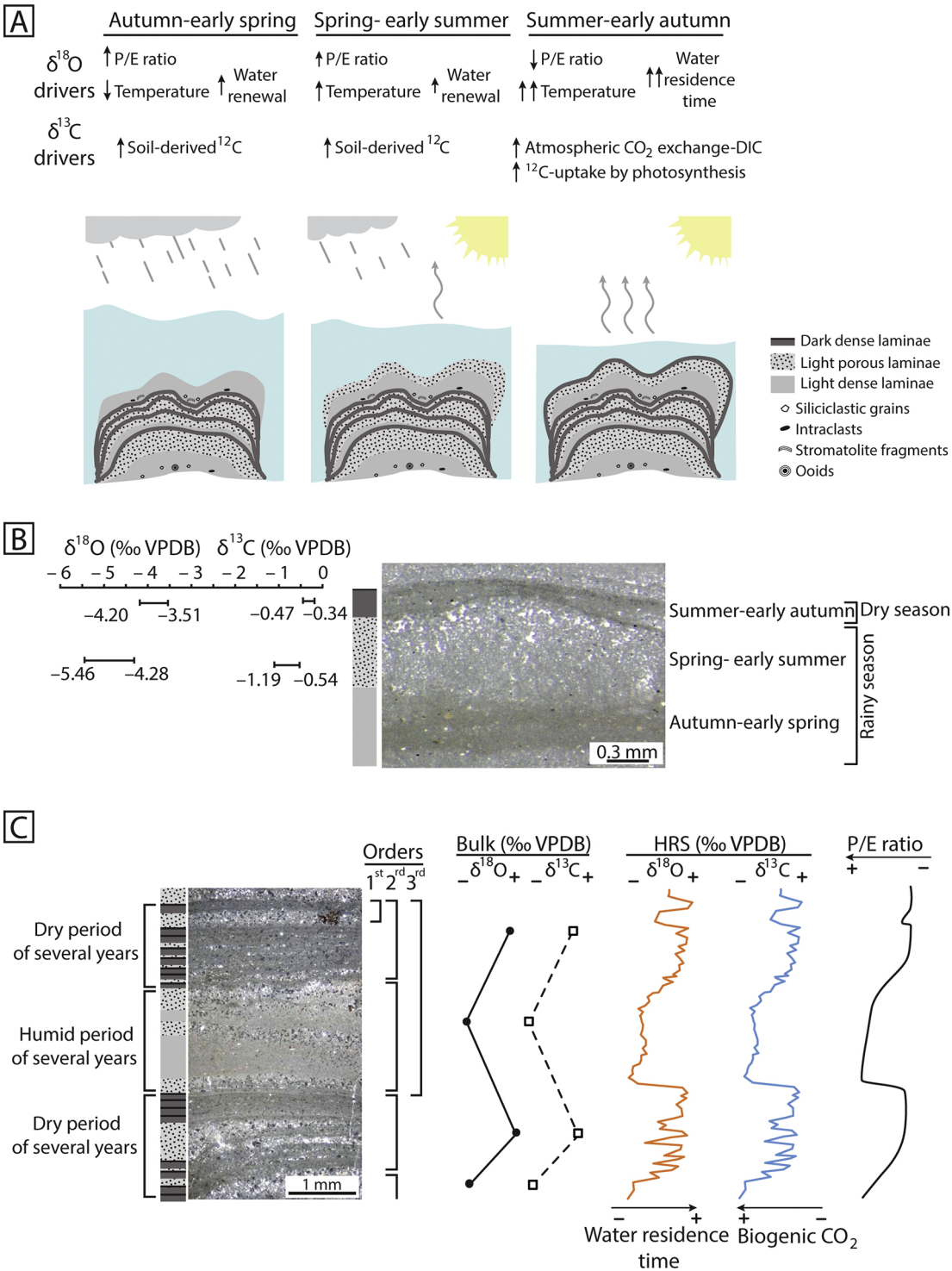
A
Autumn-early spring
Spring- early summer
Summer-early autumn
δ18O drivers
↑P/E ratio
↓Temperature
↑Water renewal
↑P/E ratio
↑Temperature
↑Water renewal
↓P/E ratio
↑↑Temperature
↑↑Water residence time
δ13C drivers
↑Soil-derived 12C
↑Soil-derived 12C
↑Atmospheric CO2 exchange-DIC
↑12C-uptake by photosynthesis
Dark dense laminae
Light porous laminae
Light dense laminae
Siliciclastic grains
Intraclasts
Stromatolite fragments
Ooids
B
δ18O (‰ VPDB)
δ13C (‰ VPDB)
−6 −5 −4 −3 −2 −1 0
−4.20
−3.51
−0.47
−0.34
−5.46
−4.28
−1.19
−0.54
0.3 mm
Summer-early autumn
Spring- early summer
Autumn-early spring
Dry season
Rainy season
C
Orders
1st 2rd 3rd
Dry period of several years
Humid period of several years
Dry period of several years
1 mm
Bulk (‰ VPDB)
− δ18O +
− δ13C +
HRS (‰ VPDB)
− δ18O +
− δ13C +
P/E ratio
+ −
− +
Water residence time
+ −
Biogenic CO2

Figure 13